1 **Genetic dissection of transcription start site selection by RNA Polymerase II in**

2 ***Saccharomyces cerevisiae***

3

4 Payal Arora[1], Kieran F. Brennan[1], Marcie H. Warner[1], Craig D. Kaplan[1]*

5

6 [1]Department of Biological Sciences, University of Pittsburgh, Pittsburgh, Pennsylvania, USA

7 *Address for correspondence: Department of Biological Sciences, University of Pittsburgh,

8 Pittsburgh, PA 15260, Life Science Annex 202, Fifth and Ruskin Avenues, Pittsburgh, PA

9 15260. Email: craig.kaplan@pitt.edu

**ABSTRACT**

Transcription initiation by RNA Pol II is driven by a preinitiation complex (PIC) comprising Pol II and general transcription factors (GTFs): TFIIA, TFIIB, TFIID, TFIIE, TFIIF and TFIIH. In *Saccharomyces cerevisiae*, transcription start site (TSS) selection proceeds by a promoter scanning mechanism where the PIC scans downstream for TSSs. To determine which factors participate in TSS selection by promoter scanning, we designed and implemented forward genetic selections using initiation-sensitive genetic reporters. These reporters were of two types, either being sensitive to upstream or downstream TSS shifts, allowing detection of alleles that affect promoter scanning in different directions. From >1000 candidates, we identified three primary classes of mutants: existing and novel mutants within known PIC components, including novel alleles of multiple TFIIH subunits; mutants that alter promoter scanning indirectly through cellular conditions (GTP levels and $Mn^{2+}$ levels); and mutants in chromatin and transcription elongation-related factors. Genome-wide analysis using TSS mapping shows that tested PIC mutants alter TSS usage globally across promoters while tested chromatin and transcription elongation mutants had much more limited effects. These studies expand the spectrum of mutants able to perturb initiation by promoter scanning and suggest potential plasticity in the TFIIH structure that may be part of the evolution of this initiation mechanism.

## INTRODUCTION

Transcription initiation in eukaryotes requires assembly of a large pre-initiation complex (PIC) comprising RNA Polymerase II (Pol II) and general transcription factors (GTF) (CONAWAY AND CONAWAY 1993; ORPHANIDES *et al.* 1996; ROEDER 1996; KORNBERG 2007). Together these components, in conjunction with transcriptional activators and coactivators effect promoter DNA opening, identification of the transcription start site (TSS), and de novo initiation of RNA synthesis using DNA-templated NTP substrates (KAPLAN 2013; ROEDER 2019). Additionally, a large number of other factors are recruited to promoters, including chromatin remodelers and factors functioning in the transition from initiation to elongation (RANDO AND WINSTON 2012). During PIC assembly, TBP and TFIIB bind to the core promoter transiently with TFIIA stabilizing TBP-DNA interactions. Pol II is then recruited to core promoter along with GTFs TFIIF and TFIIE stabilizing the TFIIB-TBP-DNA interactions. Thereafter, TFIIH is recruited into the PIC to drive open complex formation (promoter melting) and subsequent transcription initiation (BAEK *et al.* 2021).

In eukaryotes, the majority of promoters specifies multiple TSSs. In most eukaryotes, a TSS is stereotypically positioned approximately 30-31 basepairs downstream from a site of TBP binding (a canonical TATA-box or otherwise AT-rich sequence) (LIFTON *et al.* 1978; BREATHNACH AND CHAMBON 1981; DUDNYK *et al.* 2024). It is proposed that each TSS is supported by an associated PIC assembly point upstream (KADONAGA 1990; SMALE AND KADONAGA 2003; SANDELIN *et al.* 2007; KADONAGA 2012; VO NGOC *et al.* 2017a; VO NGOC *et al.* 2017b; LUSE *et al.* 2020; DUDNYK *et al.* 2024). In contrast, transcription initiation in the budding yeast *Saccharomyces cerevisiae* occurs through a promoter scanning mechanism (GIARDINA AND LIS 1993; KUEHNER AND BROW 2006; FAZAL *et al.* 2015; QIU *et al.* 2020). The driving factors for this novel initiation mechanism can only be speculated upon but given the loss of most splicing in budding yeast and its highly compact genome, scanning may allow for 5′ UTR diversification that cannot be accomplished by alternative splicing coupled to alternative

53 promoter usage. Intriguingly, PIC components and their assembled structure are highly
54 conserved between yeast and humans (BURATOWSKI *et al.* 1988; HE *et al.* 2016; AIBARA *et al.*
55 2021; SCHILBACH *et al.* 2021; TOMKO *et al.* 2021). While DNA melting by the yeast PIC occurs
56 proximal to its site of binding as in other eukaryotes (GIARDINA AND LIS 1993), the yeast PIC
57 scans downstream for TSSs, which are generally located 40-120 bp or further downstream of
58 the TATA box, when present (STRUHL 1987; PARK *et al.* 2014; LU AND LIN 2019; LU AND LIN
59 2021). TFIIH, required for Pol II promoter DNA opening in all eukaryotes, is proposed to use its
60 DNA translocase activity to continue pumping downstream DNA into the Pol II active site to
61 enable promoter scanning and usage of downstream TSSs (HAMPSEY 2006; MILLER AND HAHN
62 2006; FAZAL *et al.* 2015; FISHBURN *et al.* 2015).
63 Promoter scanning identifies TSSs based on their inherent sequence characteristics
64 together with the contributions of initiation factor and Pol II activities. Yeast share a universal
65 eukaryotic preference for $Y_{-1}R_{+1}$ as TSSs initiating at a purine (R, representing A or G), have a
66 pyrimidine (Y, representing C or T) just upstream of the TSS, and with an additional species-
67 specific contribution of the -8 position and of additional bases (HUROWITZ AND BROWN 2003;
68 ZHANG AND DIETRICH 2005; MIURA *et al.* 2006; NAGALAKSHMI *et al.* 2008; ARRIBERE AND GILBERT
69 2013; PELECHANO *et al.* 2013; MALABAT *et al.* 2015; LU AND LIN 2019; QIU *et al.* 2020; LU AND LIN
70 2021; ZHU *et al.* 2024). Scanning in yeast was conceptualized by Kuehner and Brow (KUEHNER
71 AND BROW 2006) where TSSs have innate efficiencies of usage, and the alteration of initiation
72 factor activity can alter individual TSS usage and the distribution of TSS usage at promoters
73 (KUEHNER AND BROW 2006; QIU *et al.* 2020; ZHAO *et al.* 2021). Genetic and molecular
74 experiments have shown that TSS selection in yeast is sensitive to mutation in multiple PIC
75 components (*e.g.* Pol II and GTFs (PINTO *et al.* 1992a; PINTO *et al.* 1994; FAITAR *et al.* 2001;
76 GHAZY *et al.* 2004; FREIRE-PICOS *et al.* 2005; KHAPERSKYY *et al.* 2008; JIN AND KAPLAN 2014;
77 QIU *et al.* 2020; ZHAO *et al.* 2021) and PIC-associated components (*e.g.* the conserved factor
78 Sub1, which is the yeast homolog of PC4 (KNAUS *et al.* 1996; WU *et al.* 1999; SIKORSKI *et al.*

2011; BRABERG *et al.* 2013). Mutations in the active site of Pol II that increase Pol II catalytic activity in vitro increase efficiency of initiation at each available TSS (KAPLAN *et al.* 2012; JIN AND KAPLAN 2014; QIU *et al.* 2020). With each TSS being more efficient in promoting initiation, the flux of scanning Pol II can be exhausted earlier than WT, leading to an observed upstream shift in observed TSS usage (KUEHNER AND BROW 2006; QIU *et al.* 2020). Similarly, decrease in Pol II catalytic activity causes reduced efficiency of individual TSSs, resulting in increases in the flux of scanning Pol II reaching downstream positions, and an observed downstream shift in TSS usage (KUEHNER AND BROW 2006; QIU *et al.* 2020).

In contrast to Pol II, because TFIIH is hypothesized to drive scanning through its Ssl2 translocase subunit (FAZAL *et al.* 2015; FISHBURN *et al.* 2015; TOMKO *et al.* 2017; TOMKO *et al.* 2021; ZHAO *et al.* 2021), the effects of mutations in Ssl2 on TSS distributions have been interpreted as being due to altered TFIIH processivity (ZHAO *et al.* 2021). *ssl2* alleles that confer downstream shifts in TSS distributions have been interpreted as increasing scanning processivity due to a higher probability of scanning reaching downstream positions. In contrast, *ssl2* alleles that confer upstream shifts in TSS distributions appear to do so by limiting scanning processivity, meaning that downstream positions are reached at a lower probability (KUEHNER AND BROW 2006; ZHAO *et al.* 2021). While TFIIH and Pol II are the primary activities driving TSS selection, how GTFs contribute to either efficiency or processivity pathways or through additional mechanisms is not known (JIN AND KAPLAN 2014; QIU *et al.* 2020).

Mutations in other GTFs like TFIIB (PINTO *et al.* 1992a; PINTO *et al.* 1994; BANGUR *et al.* 1997; PARDEE *et al.* 1998; FAITAR *et al.* 2001; JIN AND KAPLAN 2014) and TFIIF (SUN AND HAMPSEY 1996; GHAZY *et al.* 2004; JIN AND KAPLAN 2014) also affect TSS distributions, and among those tested, to do so genome wide (QIU *et al.* 2020; BASNET *et al.* 2026), as do tested Pol II and *ssl2* alleles of TFIIH (QIU *et al.* 2020; ZHAO *et al.* 2021). Mutations in TFIIB cause downstream shifts to TSS usage in ways that appear consistent with both TFIIB and the Pol II active site determining initiation efficiency at all TSSs (WU *et al.* 1999; FAITAR *et al.* 2001;

105 KOSTREWA *et al.* 2009; JIN AND KAPLAN 2014; QIU *et al.* 2020). Additionally, published mutations
106 in TFIIF, the GTF recruiting Pol II to the core promoter, have also been shown to shift TSSs
107 upstream (SUN AND HAMPSEY 1995; GHAZY *et al.* 2004; FREIRE-PICOS *et al.* 2005; JIN AND
108 KAPLAN 2014; QIU *et al.* 2020). Because specific alleles of TFIIF and TFIIB have been found to
109 mutually suppress each other (GHAZY *et al.* 2004; FREIRE-PICOS *et al.* 2005) and also additively
110 interact with Pol II alleles (JIN AND KAPLAN 2014; QIU *et al.* 2020), we have proposed that at
111 least some TFIIF mutants affect TSS selection by functioning alongside the Pol II active site in
112 promoting initiation efficiency (GHAZY *et al.* 2004; FREIRE-PICOS *et al.* 2005; JIN AND KAPLAN
113 2014). The interface between Pol II and TFIIH is also important for scanning and has been
114 proposed to be a key factor in the evolution of the scanning mechanism (YANG *et al.* 2022;
115 YANG *et al.* 2024; BASNET *et al.* 2026). TFIIH is tethered to the PIC via the RING finger domain
116 of Tfb3 (TFIIK kinase subdomain of TFIIH) through interactions with TFIIE and the Rpb7 subunit
117 of Pol II (SCHILBACH *et al.* 2017; YANG *et al.* 2022; YANG *et al.* 2024). In yeast, mutations in both
118 Rpb7 (BRABERG *et al.* 2013) and Tfb3 (YANG *et al.* 2024) can confer upstream shifts to TSS
119 usage *in vivo*, consistent with a defective scanning process (BASNET *et al.* 2026). Factors
120 outside of PIC such as chromatin and elongation factors have also been implicated to affect
121 promoter choice and potentially TSS selection.
122 PIC factors (Pol II and GTFs) and PIC-associated factors like Sub1 have been
123 genetically identified as contributing to TSS-selection during promoter scanning. What is not
124 known is how many additional factors might also contribute to the process of TSS selection. Are
125 there additional factors that cooperate or contribute to TSS selection but have not been
126 structurally located in the PIC akin to Sub1? What are the surfaces and networks within the PIC
127 that contribute to TSS selection by promoter scanning? Finally, promoter chromatin structure
128 can easily be imagined to affect PIC function and TSS distribution profiles because most yeast
129 promoters have TSSs that map within boundaries of the +1 nucleosome (RANDO AND WINSTON
130 2012). We have aimed to take an unbiased approach to identify any additional factors that

131 participate in TSS selection during initiation by promoter scanning using forward genetic
132 selections (BROW 2019; WANG *et al.* 2025). Through the use of existing (BERROTERAN *et al.*
133 1994) and novel genetic reporters, we have identified ~300 mutations in proteins within and
134 outside the PIC affecting TSS selection, including a number of alleles of Pol II
135 elongation/chromatin genes, *eg. SPT2, SPT4, SPT5, SPT6, SPT16, SPN1, BUR2*, and
136 histones. We then examined a subset of the novel alleles in genetic interaction studies to probe
137 relationships between mutant alleles. Finally, we examined the genome-wide effects of selected
138 PIC and chromatin/elongation-class alleles for effects on TSS-selection. We have found that
139 tested GTF alleles alter TSS usage genome wide as predicted from effects on promoter
140 scanning in general. In contrast, chromatin or Pol II elongation-class alleles did not show similar
141 widespread effects. We interpret this class of mutant as acting on TSSs in a promoter-selective
142 fashion.
143

144 **MATERIALS AND METHODS**

145 **Yeast strains and oligos**

146 Yeast strains and oligos used in this study are listed in **Table S2**.

147 **Yeast media**

148 Yeast media used in the current studies have been prepared as previously described in
149 (AMBERG *et al.* 2005; KAPLAN *et al.* 2012; JIN AND KAPLAN 2014; MALIK *et al.* 2017; ZHAO *et al.*
150 2021). Briefly, all solid media contain 2% w/v agar (BD); YPD is 1% w/v yeast extract (Gibco™
151 Bacto™), 2% w/v peptone (Gibco™ Bacto™) and 2% w/v glucose (VWR) supplemented with
152 0.15 mM adenine (Sigma) and 0.4 mM tryptophan (Sigma) for solid medium (not supplemented
153 when liquid); YPD+3% formamide contains 3% v/v formamide (Ambion); YP Raffinose (YPRaf)
154 and YP Raffinose Galactose (YPRafGal) contain 2% w/v raffinose (Amresco) (YPRaf) or 1% w/v
155 galactose (Sigma) and 2% w/v raffinose (YPRafGal). Both YPRaf and YPRafGal are additionally
156 supplemented with 1 µg/ml of (Sigma) Antimycin A to prevent aerobic respiration. Synthetic

157 minimal media (SC-) were what is referred to as “Hopkins mix” with minor alterations as
158 previously noted (AMBERG *et al.* 2005; KAPLAN *et al.* 2012) (amino acid dropout mix, 0.17% w/v
159 yeast nitrogen base w/o amino acids and 0.5% w/v ammonium sulphate (BD), 2% glucose), with
160 the appropriate dropouts. Mycophenolic acid (MPA) (ThermoScientific chemicals) containing SC
161 media were supplemented at 20 µg/ml. Other drugs in the respective media were: G418
162 (GoldBio) and clonNAT (GoldBio) at 200 µg/ml, hygromycin (GoldBio) at 300 µg/ml and
163 canavanine (Sigma) at 60 µg/ml. Synthetic minimal media containing G418, clonNAT or
164 hygromycin are prepared as above with 0.1% w/v of monosodium glutamate (MSG) replacing
165 ammonium sulphate. Drug 3-aminotriazole (3AT) (Sigma) a competitive inhibitor of His3p was
166 used in some SC-His media at varying concentrations (later noted), for setting the threshold for
167 a visible $His^+$ phenotype.

168 **Genetic selections**

169 Each of the genetic selection strains possessing initiation reporters was grown overnight in
170 liquid YPD. Cultures were then washed twice in sterile distilled water to remove residual amino
171 acids before plating on respective selection media. Selection media for the reporters were SC-
172 His + 2mM 3AT for *imd2Δ::HIS3* and SC-His + 0.1mM 3AT for *cyc1-1019::HIS3*, *adhΔ50::HIS3*
173 and *hmo1Δ38::HIS3*. For dual selection of $His^+$ $Lys^+$ candidates for downstream reporters,
174 conditions used were SC-His-Lys +5mM 3AT for *imd2Δ::HIS3* SC-His-Lys +0.1mM 3AT, Cells
175 were spread using sterile 3mm glass beads at $10^8$ cells per plate. Multiple colonies of each
176 parent strain were inoculated for genetic selection to increase chances of independent
177 candidates. Plates were then kept in a lightly sealed plastic bag to prevent drying out and
178 incubated at 30˚C for ~7 days until suppressor colonies appeared.

179 **Single spot phenotyping**

180 Suppressor candidates were picked from selection plates and spotted onto solid YPD petri plate
181 in 8x6 grid (48-well format) containing 2 parents and 46 candidates apiece for the purpose of
182 candidate rescreening and additional phenotyping. Briefly, after growth on YPD, cells were

183 transferred into 100 µl of sterile distilled water in a 96-well tray using a 48-pin replicator,
184 followed by a second dilution of 6 µl of this cell suspension into 150µl of water. A sterilized 48-
185 pin replicator was then used to spot from the 150µl cell suspension onto phenotyping media.
186 Phenotype scoring timing was day 2 for YPD 30˚C and YPD 37˚C, day 3 for YPD+3%
187 formamide and synthetic complete medium (SC), day 4 for YPRaf, day 5 for SC-Lys and YPD at
188 16˚C and day 6 for YPRafGal. Reporter phenotypes on SC-His +/- 3AT were scored on days 3
189 through 5 depending on strength and SC-His-Lys +/- 3AT on day 5. **Scoring:** Scoring was
190 performed as in (JIN AND KAPLAN 2014). Single phenotype spots were given scores from 0 to 5,
191 where 0 means no growth and 5 is WT parent growth on complete medium. For conditional
192 phenotypes where growth is indicative of mutant phenotype (i.e. $Spt^-$ phenotype or $His^+$
193 phenotypes in reporter strains), scoring was 0 for no growth (WT) with positive numbers
194 indicating increasing growth reflecting strength of mutant phenotype. Relative scores of mutants
195 were first calculated per condition by $Score_{mutant}$-$Score_{WT}$ (Relative $score_{mutant:\ condition}$). These
196 relative scores were then corrected to respective control growth condition for estimating mutant
197 score corrected to control condition (e.g.: Relative $score_{mutant:\ YPRafGal}$ - Relative $score_{mutant:\ YPRaf}$).
198 These would assign positive values to mutants where growth is better than WT, negative to
199 those where growth is worse in an any condition and a 0 to WT.
200 **Mutation validation by re-introduction:**
201 Mutations were reintroduced into a clean parental strain possessing relevant initiation reporter
202 to validate effects of candidate mutations on reporter expression. Mutations were amplified from
203 suppressor strains and fused with a drug resistance marker by PCR sewing to generate a
204 *mutation::drug resistance marker* cassette and reintroduced into parent strains (JANKE *et al.*
205 2004). The marker used was *kanMX6* containing an insulated resistance cassette (pFA6a-
206 KanMX6-ins2, Addgene 195039) to minimize potential effects of marker expression on adjacent
207 loci (POWERS *et al.* 2022). Multiple independent transformants were phenotyped and genotyped
208 to assess correlation of reporter suppression and introduction of the mutant genotype along with

209 the resistance marker. The marker was also used to tag mutation loci to enable synthetic
210 genetic array analysis and selection of mutant loci through genetic crosses. CRISPR based
211 mutagenesis was performed to generate *rpb10* and *tfg1* mutations in the genome as described
212 in (LAUGHERY *et al.* 2015).

213 **Diploid generation**

214 Complementation assays and genetic interaction studies were performed with diploid
215 generation. Diploids were generated by mating suppressor candidates against parent or mutant
216 strains of opposite mating type, followed by double selection of individual haploid markers for
217 selecting diploids. Briefly, candidate suppressors, pre-integrated with auxotrophic markers
218 (*LEU2* for *MATalpha* and *TRP1* for *MATa*) were mated with the opposite mating type of the
219 required strains with a second auxotrophic selection marker; or appropriate drug resistance
220 markers were used for diploid selection for genetic interactions. Mating was performed by
221 transferring solid YPD-grown candidates to pre-aliquoted 100 µl-per-well of saturated culture of
222 test strain per well in a 96-well plate using a 48-pin (8x6) replicator and spotting onto solid YPD
223 using the same replicator. Post incubation for 2 days at 30˚C on plates, cells were transferred
224 into 100µl of pre-aliquoted sterile distilled water with the 48-pin replicator and resuspended by
225 shaking of replicator followed by transfer onto a double-selection media. These were incubated
226 at 30˚C to select for diploids for 2 days.

227 **Double mutant generation by synthetic genetic array**

228 Double mutants were generated from diploids of "tagged" single mutants mated in high
229 throughput following protocol from the Boone lab
230 (https://boonelab.ccbr.utoronto.ca/pdf/SGA_protocol_final.pdf). Briefly, a panel of *MATα single*
231 *mutation 1::drug resistance marker 1* strains was mated to a query *mutation 2::drug resistance*
232 *marker 2 MATa* strain possessing a *MATa* marker *can1Δ::STE2pr-URA3,* and diploids were
233 selected by double drug resistance as mentioned. After two days of incubation on double drug
234 diploids were transferred from solid medium directly onto solid enriched sporulation media (1%

235 potassium acetate enriched with auxotrophic amino acids in 2% agar) for 5 days at 27˚C. After
236 sporulation, sporulated spots were transferred into 50 µl sterile distilled water in 96 well plate
237 using a pinner, resuspended and spotted onto haploid selection media (SC-Ura-
238 Arg+MSG+canavanine), single mutant selection media (SC-Ura-Arg+MSG+canavanine + drug
239 1 or drug 2) and double mutant (SC-Ura-Arg+MSG+canavanine+drug 1+drug 2) selection media
240 in parallel instead of the traditional approach where mutants (single or double) are selected after
241 *MATa* meiotic progeny selection in tandem. We have observed that sicker haploids are lost if
242 selections are performed in tandem.

243 **Genomic DNA sequencing**

244 Candidate mutations were identified via AmpliSeq-based custom amplicon sequencing or whole
245 genome sequencing (WANG *et al.* 2025). Genomic DNA was isolated from candidates using
246 PureLink™ Pro 96 Genomic DNA Purification Kit and YeaStar genomic DNA kit from Zymo
247 research for AmpliSeq based sequencing. The Plasmid miniprep kit from Zymo research,
248 customized with bead lysis was used for genomic DNA isolation for whole genome sequencing.
249 AmpliSeq libraries were prepared and sequenced by the Texas A&M TIGGS genomics core
250 facility. AmpliSeq libraries were prepared following AmpliSeq for Illumina protocol for a custom
251 oligo pool comprising 1917 encompassing 310 genes. These genes comprise ORFs of
252 transcription machinery and transcription-associated genes. Libraries were sequenced in
253 batches of 96 samples using full Illumina MiSeq of 15 million reads by 250bpx2 run to aim for an
254 average coverage of ~80X per amplicon. Whole genome sequencing of samples was performed
255 by Seqcoast or Seqcenter. Each genomic DNA sample was sequenced at a depth of 400Mbp
256 yielding an average coverage of ~30X.

257 **AmpliSeq data processing**

258 Paired-end sequencing fastq files were first trimmed for adaptors at the 3′ end, followed by 3′
259 and 5′ oligo trimming (amplification oligos do not contribute towards mutation detection) by
260 cutadapt v2.1 (MARTIN 2011). These were then processed by MutantHuntWGS v1.1 (ELLISON *et*

261 *al.* 2020), a container-based package deploying predefined tools for alignments and variant
262 calling. Briefly, oligo and adaptor-free paired-end fastq files were aligned to *Saccharomyces*
263 *cerevisiae* S288C reference genome R64-2-1 by bowtie2 v2.2.9 (LANGMEAD AND SALZBERG
264 2012) resulting in bam alignment files followed by bam sorting and indexing by SAMtools v1.3.1
265 (LI *et al.* 2009; DANECEK *et al.* 2021). Genotype likelihoods were calculated followed by variant
266 calling by BCFtools v1.3.1 (DANECEK *et al.* 2021) using haploid ploidy file provided by
267 MutantHuntWGS v1.1 (ELLISON *et al.* 2020) (ELLISON *et al.* 2020). This resulted in vcf files for all
268 sequenced candidates. Mutant variants in mutant vcf files were differentially called relative to
269 parent vcf files by VCFtools v 0.1.14 (DANECEK *et al.* 2011). Resulting differential mutants were
270 annotated using SNPeff v4.3p (CINGOLANI *et al.* 2012) and SIFT4G (VASER *et al.* 2016), which
271 uses EF4.74 *Saccharomyces cerevisiae* library for annotating severity of amino acid change.
272 For WGS, fastq reads were analyzed by Seqcenter and Seqcoast for mutation detection by
273 breseq (DEATHERAGE AND BARRICK 2014). *Saccharomyces cerevisiae* S288C reference genome
274 R64-1-1 was used for annotation which generated a list of variants. Variants specific to
275 suppressor candidate were curated by a custom shell script comparing mutant variants to
276 parent variants.

277 **STRIPE-seq**

278 Total RNA was isolated from 50 mL of mid-log yeast culture with density of $1X10^7$ cells/mL as
279 described previously (SCHMITT *et al.* 1990) and resuspended in 90 µL nuclease free water. RNA
280 samples were in-column DNase I treated using the RNeasy mini kit from Qiagen with 100 µg
281 RNA input per column. DNased RNAs (10 µg per sample) were depleted of rRNA using
282 bioltinylated riboPOOL kit for *Saccharomyces cerevisiae* from siTOOLS Biotech, purified by
283 Dynabeads MyOne Streptavidin C1 and eluted in 9 µL nuclease free water. STRIPE-seq
284 libraries were then generated from rRNA depleted RNAs using 200 ng RNA per sample as
285 previously published (POLICASTRO *et al.* 2020) with our modifications. Briefly, 200 ng of each
286 RNA sample, split into two 100 ng reactions were terminator exonuclease (TEX) treated to

287 remove uncapped RNA. Pooled, TEXed reactions were then reverse transcribed using a
288 random 10-mer with partial homology to P7 adaptor RTO
289 (GCCTTGGCACCCGAGAATTCCANNNNNNNNNN) instead of a complete P7:oligo-random
290 pentamer (modification; P7 adaptor added during final library amplification). Non-templated
291 cytosines at the 3′ end of cDNA then allow annealing of a template switching oligo, containing
292 partial P5 adaptor, 9-base UMI (instead of 8-base UMI) and a linker (TATAGGG) (Biotin-
293 GTTCAGAGTTCTACAGTCCGACGATCNNNNNNNNNTATArGrGrG). After template switching,
294 libraries were amplified by dual indexing primers with complete P5 and P7 adpaters. Libraries
295 (>200-800 bp) were extracted from 3% polyacrylamide TBE gel to remove oligos and then
296 sequenced by Illumina NextSeq 2000 system with 1X50 bp sequencing cycle. Sequencing
297 reads were delivered demultiplexed.

298 **STRIPE-seq analysis**

299 STRIPE-seq fastq files were processed as TSS-seq reads we had previously published (ZHAO
300 *et al.* 2021) with STAR alignment and additional bam processing followed previously published
301 of goSTRIPES and TSRexploreR packages (POLICASTRO *et al.* 2020; POLICASTRO *et al.* 2021;
302 POLICASTRO AND ZENTNER 2022). Fastq files were filtered for quality with fastx-toolkit v 0.0.14 (-
303 q 20 -p 75) (http://hannonlab.cshl.edu/fastx_toolkit/), followed by trimming of adaptors by
304 trimmomatic v 0.38 (BOLGER *et al.* 2014) and then 9 base UMI extraction by umi-tools v 1.0.0
305 (SMITH *et al.* 2017). Reads were then trimmed of linker TATAGGG and then trimmed to 25
306 bases by cutadapt v 2.10 (MARTIN 2011) before local alignment by STAR v 2.7.9a (DOBIN *et al.*
307 2013) generating bam files. Bam files with uniquely mapping reads were then filtered of
308 unfavorably flagged reads by samtools v 1.9 (samtools view –F 3844) (LI *et al.* 2009; DANECEK
309 *et al.* 2021) followed by deduplication by umi-tools v 1.0.0 (SMITH *et al.* 2017). Deduplicated and
310 indexed bam files were then processed by the protocol followed by the Zentner lab (POLICASTRO
311 *et al.* 2020; POLICASTRO *et al.* 2021; POLICASTRO AND ZENTNER 2022). Briefly, reads with more
312 than 3 soft-clipped 5′ bases are listed and filtered out by picard v 2.18.12 (Picard Toolkit 2019)

313 following GoSTRIPES (Robert Policastro). Indexed filtered bams were then processed by
314 TSRexploreR (POLICASTRO *et al.* 2021) for G correction to generate bedgraphs for 5′ ends of
315 reads (TSSs) that we processed to split into + and – strand bedgraphs and downstream
316 analyses following our TSS-seq pipeline (ZHAO *et al.* 2021). Pearson correlation matrices were
317 generated for bedgraphs of all libraries using our in-house Rscript. Promoter matrices
318 representing TSSs were generated comprising 401 base window (250 bases upstream and 150
319 bases downstream from median TSS position including the median) across 5979 annotated
320 promoters (RHEE AND PUGH 2012). These matrices were utilized for estimating median and
321 spread (base distance between $10^{th}$ and $90^{th}$ percentile) of TSS distributions across the 5979
322 promoter and eventually Δmedian and Δspread of mutants relative to WT for differences (ZHAO
323 *et al.* 2021). Promoter matrices were row normalized before generating average matrices across
324 replicates and estimating average median and average spread values for calculating average
325 Δmedian and Δspread values relative to average WT. Top 2829 promoters with expression
326 cutoff of 10 were selected based on library normalized average of all WTs sorted by expression:
327 sum of TSSs per 401 base promoter window.
328

329 **RESULTS**

330 **TSS-shifting mutants identified by transcription initiation genetic reporters**

331 To understand the genetic requirements for initiation by promoter scanning, we established
332 genetic selection systems for the isolation of transcription start site-shifting mutants. We
333 deployed four initiation reporter alleles designed or chosen because expression from the
334 reporter is sensitive to altered TSS selection: *imd2Δ::HIS3, cyc1-1019::HIS3*, *adhΔ50::HIS3,*
335 and *hmo1Δ38::HIS3* (**Fig. 1**). These reporters comprise native (*imd2Δ::HIS3*) (MALIK *et al.* 2017)
336 or engineered (*cyc1-1019::HIS3*, *adhΔ50::HIS3* and *hmo1Δ38::HIS3*) (FURTER-GRAVES AND
337 HALL 1990; PINTO *et al.* 1992a; PINTO *et al.* 1992b) promoters that have each been fused to the
338 *HIS3* ORF. In wild type cells, they generally do not express sufficient levels of *HIS3* gene

339 product to confer growth on medium lacking histidine (the His$^-$ phenotype). In the presence of a
340 TSS selection mutant conferring an upstream or downstream shift appropriate to the reporter
341 configuration, a shift in TSS usage leads to expression of a functional *HIS3* mRNA, allowing
342 cells to grow on medium lacking histidine (the His$^+$ phenotype) (**Fig. 1a**). We tuned our
343 phenotypic selections through the use of the drug 3-aminotriazole (3AT), a competitive inhibitor
344 of His3p (KLOPOTOWSKI AND WIATER 1965; STRUHL AND DAVIS 1977), allowing a shift in the
345 threshold of reporter activity needed to confer the His$^+$ phenotype and beneficial for reporters
346 that allowed leaky *HIS3* expression in WT cells (**Fig. 1b**). We reasoned that using two different
347 promoters for each class of TSS-shift reporter would allow us to prioritize mutants more likely to
348 affect promoter scanning globally as opposed to reporter-specific alleles. We previously
349 developed and characterized the *imd2Δ::HIS3* reporter where *HIS3* replaces the *IMD2* ORF and
350 is under control of the *IMD2* promoter (MALIK *et al.* 2017). Downstream shifts to TSS usage
351 bypass a terminator element in the *IMD2* promoter and allow expression of the downstream
352 ORF (KOPCEWICZ *et al.* 2007; JENKS *et al.* 2008; KUEHNER AND BROW 2008). We found this
353 reporter exquisitely sensitive to defects in Pol II and GTFs leading to downstream TSS shifts
354 (MALIK *et al.* 2017) and also that we could identify alleles of *SSL2* (ZHAO *et al.* 2021) or *TFA1*,
355 *TFB3*, or *RPB7* (BASNET *et al.* 2026) able to suppress this reporter through genetic screens or
356 site-directed mutagenesis. Therefore, this reporter appears sensitive to mutations in multiple
357 PIC components that might each alter promoter scanning in distinct ways, *i.e.* controlling Pol II
358 initiation efficiency or controlling scanning processivity.
359 Our other downstream shift-detecting reporter *cyc1-1019::HIS3* functions analogously to
360 *imd2Δ::HIS3* (NA *et al.* 1992; PINTO *et al.* 1992a; PINTO *et al.* 1992b). Here, downstream shifts in
361 TSS usage allow bypass of an introduced upstream ATG (the *cyc1-1019* allele). The introduced
362 ATG allows translation initiation out of frame with *HIS3* and confers a His$^-$ phenotype. Shift to
363 use of downstream TSSs allows translation to begin at the normal *HIS3* ATG. A variant of this
364 reporter configuration (*cyc1-5000*) was used to identify the first *SUA7* (TFIIB) alleles (PINTO *et*

365 *al.* 1992a; PINTO *et al.* 1992b) as well as alleles of *RPB1* (*SUA8*) (BERROTERAN *et al.* 1994).
366 This reporter is less leaky than *imd2Δ::HIS3* and thus more tightly His$^-$ even in the absence of 3-
367 AT (**Fig. 1b**). We demonstrated that strong downstream shifting mutants *rpb1* H1085Y and
368 *sub1Δ* were His$^+$ using this reporter (**Fig. 1b**).
369 Our upstream shifting reporters function analogously to each other. In each case, a
370 reduced TSS to ATG distance likely hampers translation initiation of *HIS3* because the *HIS3*
371 ATG is too close to the 5′ end of the mRNA (FURTER-GRAVES AND HALL 1990). 5′ extension of
372 the mRNA through usage of an upstream TSS allows more efficient *HIS3* translation initiation.
373 We employed *adh50Δ::HIS3*, previously shown to detect *rpb9* alleles as upstream shifters
374 (FURTER-GRAVES AND HALL 1990; FURTER-GRAVES *et al.* 1991), and a second, novel upstream
375 reporter. To create an additional upstream shift-detecting reporter, we analyzed our previous
376 genome wide TSS data (QIU *et al.* 2020) for promoters that showed especially large shifts in
377 TSS usage in response to upstream TSS mutants, settling on *HMO1*. We then fused different
378 lengths of the *HMO1* promoter, truncated by 38, 45 and 53 basepairs to *HIS3* to ask if any of
379 these configurations could cleanly detect upstream TSS-shifting mutants (**Fig. S1a**). First, we
380 tested if these variants could function effectively as potential initiation reporters by assessing if
381 they showed suppressibility when exposed to UV mutagenesis (**Fig. S1a**), an approach
382 previously tested for reporter suppressibility (HAMPSEY 1991). After observing reporter
383 suppressibility, we tested them in conjunction with TSS-shifting Pol II and *rpb9* mutants (**Fig.**
384 **1b**).
385
386 **Identification of novel upstream and downstream TSS-shifting mutants**
387 For our selections, we integrated our engineered reporters (*cyc1-1019::HIS3*, *adhΔ50::HIS3* and
388 *hmo1Δ38::HIS3*) at a gene-free locus on chromosome I (**Fig. S1b**) (GRUBER *et al.* 2012) with
389 *imd2Δ::HIS3* present at the native *IMD2* locus. We isolated suppressors of initiation reporters by
390 genetic selection of His$^+$ candidates and did so in two batches with two versions of genetic

391 selection strains. In an initial pilot genetic selection, ~700 candidates were isolated across the
392 four first generation strains carrying the reporters described above, with the majority isolated
393 from the *IMD2* reporter. Candidates were re-phenotyped for their $His^+$ phenotypes and for
394 secondary conditional or transcription-related phenotypes. These included growth on YPD at
395 30 °C, 16 °C, 37 °C and with 3% formamide, SC supplemented with MPA to detect MPA
396 sensitivity commonly observed for known upstream shifting TSS alleles (ZHAO *et al.* 2021), SC-
397 Lys medium to test for suppression of the $Spt^-$ reporter allele *lys2-128∂* (SIMCHEN *et al.* 1984;
398 CUI *et al.* 2016), and YPRafGal with YPRaf as a control for suppression of *gal10Δ56* (GREGER
399 AND PROUDFOOT 1998; GREGER *et al.* 2000; KAPLAN *et al.* 2005), a reporter allele able to detect
400 different kinds of transcription-associated phenotypes. We utilized profiles of phenotypes to
401 potentially cluster mutants by similarity of their additional phenotypes and to choose candidates
402 from distinct phenotypic groups for further study. Additionally, known phenotypes of existing
403 mutants allowed provisional attribution of candidates to possible candidate genes. We chose
404 168 of these candidates for sequencing using a custom Illumina AmpliSeq amplicon pool (WANG
405 *et al.* 2025). Of 168 candidates sequenced using Illumina AmpliSeq, we identified a potential
406 causative mutation in 72 of them. For genes already linked to TSS selection, we identified
407 alleles of *SUA7* (2 unique alleles), *RPB1* (8 unique alleles), *RPB2* (8 alleles from 11
408 candidates), *RPB9* (2 unique alleles), and *SUB1* (3 alleles from 4 candidates). Because of
409 inconsistent coverage with AmpliSeq, we piloted whole genome sequencing for 10 of the initial
410 candidates where AmpliSeq failed to identify a candidate mutation. Whole genome sequencing
411 (WGS) identified potential causative mutations for 7/10 candidates sequenced and provided
412 information allowing refinement of our selection procedures as described below.
413 This preliminary analysis allowed us to refine our selections for a second round where we
414 identified additional both upstream- and downstream-shifting candidates (**Figs. 2, 3, 4, 5**). We
415 identified transcription-related mutants (subset displayed in **Figs. 2, 3, 4, S2, S3**) but also
416 identified classes of mutant that appear reporter specific (*e.g.* guanine metabolism, **Fig. 5a**) and

417 a likely indirect modulator of TSS selection (e.g. *PMR1*, **Fig. 5b**), classes that AmpliSeq would
418 have failed to identify. Candidates mutations identified by sequencing are compiled in **Table S1.**
419 Previously identified TSS shifting alleles are compiled in **Table S3**. We then incorporated
420 secondary screening to filter these latter classes out as discussed in the next section. Among
421 upstream-shifting candidates, we filtered out recessive loss of function mutants in *RPB9* by a
422 complementation assay. In a subsequent third round genetic selections we isolated ~1750 more
423 candidates comprising 447 suppressors of *imd2Δ::HIS3*, 672 of *cyc1-1019::HIS3* (**Fig. 2a**), 293
424 of *adhΔ50::HIS3,* and 350 of *hmo1Δ38::HIS3* (**Fig. 3a**) and after phenotyping-based filtering we
425 prioritized ~250 candidates for whole genome sequencing. In a separate selection of
426 *imd2Δ::HIS3* suppressors performed by the students in the BIOSC 0068 Foundations of Biology
427 Laboratory 2 course at the University of Pittsburgh, 48 $His^+$ candidates were prioritized by
428 phenotypic and genotypic screens for whole genome sequencing, yielding 46 candidates. These
429 were combined with the above 447 *imd2Δ::HIS3* suppressors amounting to 495 *imd2Δ::HIS3*
430 suppressors (**Fig. 2a**). Prioritization across all reporter classes resulted in a total of ~300
431 candidates sequenced by whole genome sequencing. Out of the ~300 candidates sequenced,
432 we identified reporter transcription-associated mutations in ~240 of these and further ~160
433 unique mutants.

434 Of all transcription-related mutants isolated in this study, we observed three primary
435 groups: PIC mutants, indirect effectors of TSS selection (*e.g. PMR1*) or promoter specific non-
436 transcription factors *e.g.* guanine mutants), and chromatin/Pol II elongation factors. We
437 validated 8 candidates through reconstruction of mutants by generating alleles in a clean
438 genetic background and all 8 recapitulated candidate suppression (**Fig. 2b**). In addition to direct
439 validation by reconstruction of a subset of mutants, several lines of evidence support the
440 mutations identified by WGS are causative for phenotypes. First, we selected spontaneous
441 suppressors, so the expectation was for most strains to have essentially a single causative

442 mutation. Second, we identified previously described alleles of *SUA7*, *RPB1*, *RPB2*, *TFB3*,
443 *SPT6*, and *TFA1* while not observing changes elsewhere in their genomes. Third, we identified
444 multiple inactivating alleles of *SUB1* and *RPB9* as expected for non-essential genes with known
445 effects on TSS selection, while not observing changes elsewhere in their genomes. Fourth,
446 there were five cases where we identified the identical allele independently in separate
447 selections. Finally, nearly all candidate sequencing data showed only a single change in a gene
448 that could rationally be linked to transcription initiation. Because previous genetic interaction
449 studies have helped annotate functions to mutations (JIN AND KAPLAN 2014; ZHAO *et al.* 2021),
450 we tested inter-subunit interface mutants and genetic interactions across a subset of our
451 mutants before assessing TSS shifts caused by our novel mutants genome wide, which we
452 discuss later.

453 Among mutants in PIC components, we identified alleles of Pol II (*RPO21/RPB1*, *RPB2*,
454 *RPB9*, *RPB10*) and of GTFs (TFIIB, *TFA1*/TFIIE, *TFG2*/TFIIF, TFIIH: *SSL2*, *SSL1*, *TFB2*, *TFB3*,
455 *TFB4* and *RAD3*) (**Fig. 4**). We first observed a high prevalence of mutations in the downstream
456 shifting class in *RPB1* and *RPB2* lining the cleft leading to and surrounding the active site.
457 Because *RPB1* and *RPB2* are larger genes, these mutants predominated in our selections,
458 though many of these mutations were novel (**Figs. 4a, b**). Because downstream shifting is
459 expected from reduced Pol II activity (KAPLAN *et al.* 2012; MALIK *et al.* 2017), catalytic or
460 structural defects that lead to reduced catalytic activity or PIC function are expected to be
461 isolated as downstream shifters. However, not all *rpb* mutants clustered around the active site
462 (**Figs. 4a, b**). We observed two types of mutations amongst those surrounding the activity cleft.
463 We found that in both Rpo21/Rpb1 and Rpb2, mutations within structural domains surrounding
464 the cleft displayed formamide sensitivity (**Fig. 4d**), a phenotype that could reflect protein folding
465 or stability defects. Mutations facing or on the surface of the cleft generally were formamide
466 resistant. We also isolated mutations at intra-subunit interfaces including those linked to control

467 Pol II catalysis. For example, we isolated an upstream-shifting mutation G707V in the Rpb1
468 anchor loop region (**Fig. 4e**). This loop lies between α20 and α21 helices of Rpb1 (KASTER *et al.*
469 2016) and a poly-alanine substitution at Rpb1 707-709 in the anchor loop was previously shown
470 to confer MPA sensitivity, consistent with an upstream shift in TSS usage (KASTER *et al.* 2016).
471 We additionally observed mutations in the Rpb1 α21 helix, A725T and E734D, both resulting in
472 downstream shifts. A prior mutation in Rpb1 α21, G730D, was identified as a reduced catalytic
473 activity mutant and appeared to function through incompatibility with Rpb9 in that slow growth of
474 G730D was suppressed by *rpb9*Δ (KASTER *et al.* 2016). It is possible that these substitutions
475 work similarly though they are predicted to be more subtle. Alternatively, E734 is positioned to
476 potentially interact with a network of residues that connects to an Rpb1-Rpb8 interaction but is
477 also adjacent to TFIIS when it is inserted into the active site. However, no role for TFIIS in TSS
478 selection has yet been described. Regardless, perturbation to E734 could result in reduced Pol
479 II catalysis, leading to a downstream shift in TSS usage.
480 Of *rpb2* mutations, beyond the active cleft, we observed mutations in Pol II-lobe-jaw
481 domain along the path of DNA entry near the Rpb9-TFIIF interface (HEMMING *et al.* 2000) (**Fig.**
482 **4f**). Because previous studies have shown that perturbation of both TFIIF and Rpb9 functions
483 results in upstream shifts (FURTER-GRAVES *et al.* 1991; HULL *et al.* 1995; SUN AND HAMPSEY
484 1995; SUN *et al.* 1996; KHAPERSKYY *et al.* 2008; EICHNER *et al.* 2010), the upstream-sensitive
485 reporter suppressor Rpb2 C317R could be consistent with disruption of this interface. Here,
486 Rpb2 C317 is buried, and substitution of an arginine might be predicted to perturb structure and
487 alter positioning of either Rpb9 or TFIIF or both. Disruption of Tfg1 at this interface
488 encompassing residue R422 (homologous to R417 in the studied *S. mikate* Tfg1) (EICHNER *et*
489 *al.* 2010) and deletion of *RPB9* (WOYCHIK *et al.* 1991) each result in a cold sensitive phenotype,
490 a phenotype shared by Rpb2 C317R (**Fig. 3b**). In contrast to Rpb2 C317R, a nearby
491 substitution E319D results in the opposite phenotype – suppression of a downstream-shift
492 sensitive reporter. While Rpb2 E319 is close to Tfg1, it appears to make direct interactions with

493 Rpb9 Y15 and R30 and perturbing the length of the 319 sidechain in E319D may alter this
494 interaction with Rpb9 (**Fig. 4e**).
495 We also isolated Rpb2 G369C and G369R mutants as upstream shifters (**Fig. 4f**).
496 Substitutions in Rpb2 G369 were previously isolated as Spt$^-$ (HEKMATPANAH AND YOUNG 1991),
497 as a suppressor of a TFIIB downstream-shifting allele (CHEN AND HAMPSEY 2004), and to be
498 MPA$^S$ with altered termination at a genetic reporter allele involving *ADH2* (KUBICEK *et al.* 2013).
499 Bulky substitutions for glycine at this residue would be in position to interfere with the Rpb1-Tfg1
500 interface (CHEN *et al.* 2007; SCHILBACH *et al.* 2021). Previous studies show that mutation in the
501 TFIIF dimerization domains within both Tfg1 and Tfg2 subunits also resulted in upstream TSS
502 shifts (SUN AND HAMPSEY 1995; GHAZY *et al.* 2004; EICHNER *et al.* 2010). Intriguingly, we also
503 isolated a downstream shifting mutation in the Pol II subunit Rpb10, a subunit shared amongst
504 the three eukaryotic nuclear RNA polymerases. This allele is discussed below where we probe
505 how this substitution may be working (**Fig. 6**).
506 Among GTFs, we identified novel alleles of *TFG2* (TFIIF), *SUA7* (TFIIB)*, RAD3, SSL1,*
507 *SSL2, TFB2*, *TFB4* and *TFB3* (TFIIH) and *TFA1* (TFIIE). For Tfg2, we identified three
508 suppressors of a downstream-shift sensitive reporter: V128G, C222Y (**Figs. 2b**, **4g**) and T366P
509 (**Table S1**) (with C222Y isolated twice). This is the first occurrence of *tfg2* alleles potentially
510 conferring downstream shifts, because previously identified mutants of Tfg2 that affected TSSs
511 resulted in upstream shifts (SUN AND HAMPSEY 1995; GHAZY *et al.* 2004; EICHNER *et al.* 2010).
512 Tfg2 V128 and C222 are close to each other in space but there is not an obvious interpretation
513 for their structural perturbations. Interestingly, while Tfg2 substitutions V128G and C222Y lie
514 within the Tfg2 dimerization domain (but not at the dimerization interface), T366P lies in the
515 winged helix domain (WH) and is not visualized in the yeast PIC. The WH domain has been
516 proposed to interact with upstream DNA (EICHNER *et al.* 2010).

517 In *SUA7,* we isolated novel suppressors of downstream-shift sensitive reporters in the B-
518 finger/B-reader domain such as R60W and G80R alleles as well as those in previously studied
519 residues R64K (BANGUR *et al.* 1997; PARDEE *et al.* 1998) and R78C (PINTO *et al.* 1994) (**Fig. 4h,**
520 **Table S1**). We note that G80R is cold sensitive just as are classical *sua7* alleles (PINTO *et al.*
521 1992b). Besides substitutions in the B-reader domain, we also identified R182C in the
522 Sua7/TFIIB B-core N-terminal cyclin fold (**Fig. S2**), the domain that interacts with the Pol II wall,
523 involved in directing the DNA-RNA hybrid (CRAMER *et al.* 2001; KOSTREWA *et al.* 2009). The
524 TFIIB B-core domain binds to the Pol II complex at the Rpb2 "wall" domain, which undergoes
525 reorganization as a consequence of the TFIIB-Pol II interaction. Previously isolated substitutions
526 in C149 at the TFIIB/Rpb2 interface resulted in a downstream TSS shift (WU *et al.* 1999). Our
527 new substitution, Sua7 R182C is in a residue that packs with Sua7 C149, which is adjacent to
528 the Rpb2 wall domain residue M868 (KOSTREWA *et al.* 2009; SAINSBURY *et al.* 2013) (**Fig. 4h**).
529 We also isolated Rpb2 substitutions in the wall near the N-terminal B-cyclin fold domain
530 proximal to M868 (Rpb2 G867S, Y931C, L961S). Unbiased isolation of TSS mutants at this
531 interface highlights the ability of our selections to identify interfaces involved in TSS selection.
532 Within TFIIH, we isolated alleles across the complex, consistent with a network of
533 interactions throughout its subunits able to modulate the scanning process. Within Ssl1, *ssl1*
534 I122T and *ssl1* R230G were isolated and are the first *ssl1* alleles directly connected to TSS
535 selection. *SSL1* was initially genetically isolated through a suppressor of a stem loop placed at
536 the 5′ UTR of *HIS4* (YOON *et al.* 1992) and potentially regulates Rad3 helicase activity involved
537 in NER (COIN *et al.* 1998; KIM *et al.* 2015) via its VWA family protein domain. Rad3 activity is not
538 implicated in TFIIH initiation functions and the location of our *ssl1* alleles suggests that they
539 might instead alter internal Ssl1 interactions or the organization of residues that interact with
540 Tfb1 or Tfb4 or both. Ssl1 I122 is directly adjacent to a loop of Tfb4 that inserts into Ssl1 while

541 Ssl1 R230 is positioned internally to organize an Ssl1 loop that connects to both Tfb1 and Tfb4
542 interfaces (**Fig. 4i**).
543 Further, we isolated Tfb2 F189S that lies in the HEAT repeats domain of Tfb2 as a
544 suppressor of a downstream shift-sensitive reporter. Tfb2 F189 contributes to hydrophobic
545 packing within Tfb2 that might limit dynamics or breathing of this critical connector protein for
546 bridging Ssl2 to the rest of TFIIH. Relaxation of this domain through loss of the bulky
547 phenylalanine sidechain potentially could confer flexibility on the connection of Ssl2 to the rest
548 of the complex (**Fig. 4k**). Similarly to how Tfb2 connects Ssl2 to the rest of TFIIH, Tfb4 is the
549 connector of Tfb2 to the rest of TFIIH. We isolated *tfb4* N71K as a suppressor of a downstream
550 shift-sensitive reporter. Tfb4 N71 lies in the VWA domain and insertion of a bulkier and charged
551 lysine into an internal Tfb4 pocket might also loosen the Tfb4 structure, potentially adding
552 flexibility to the linkages across components (**Fig. 4k**).
553 Tfb3 is critical connecting TFIIH by its RING domain to Pol II (through Rpb7) and the rest
554 of the PIC (through TFIIE). Previously tested mutations that disrupt this interface cause
555 upstream shifts in TSS selection (YANG *et al.* 2022; YANG *et al.* 2024; BASNET *et al.* 2026), while
556 removal of the Tfb3 RING domain or the TFIIK kinase module (part of TFIIH) result in usage of
557 TSSs ~30 bp downstream of the TATA box *in vitro*, similarly to non-scanning eukaryotes
558 (MURAKAMI *et al.* 2015; YANG *et al.* 2022). We have interpreted these mutants as conferring a
559 defect in scanning, either a loss of scanning processivity or reduction in scanning rate. Here, we
560 have isolated *tfb3* S23F as suppressing a downstream shift-sensitive reporter (**Fig. 4l**). Tfb3
561 residue S23 lies within the Tfb3 RING finger domain and is present in a loop adjacent to a
562 hydrophobic interface with TFIIE subunits Tfa1 and Tfa2, formed by Tfb3 L22, Tfa1 I183, Tfa1
563 V102, Tfa1 H103, and Tfa2 L283 (**Fig. 4l**). Intriguingly, a potentially more disruptive substitution
564 at the very same residue, *tfb3* S23P, was isolated as an upstream shifter along with other
565 disruptive substitutions at the Tfb3-TFIIE interface (YANG *et al.* 2022; YANG *et al.* 2024; BASNET
566 *et al.* 2026). Because it has the opposite phenotype of Tfb3 S23P, we interpret Tfb3 S23F as

567 stabilizing the Tfb3-TFIIE interaction (see Discussion). Supporting our interpretations of
568 mutations identified in targeted *TFB3* and *TFA1* genetic screens or site-directed mutational
569 studies (YANG *et al.* 2022; YANG *et al.* 2024; BASNET *et al.* 2026), we isolated mutations R64T
570 and P51L in *TFB*3 that result in suppression of upstream shift-sensitive reporters, namely Tfb3
571 R64T and P51L (**Fig. 3, 4l**). Tfb3 R64 had previously been identified as making a key interaction
572 with Rpb7 and each side of this interaction appears to function in promoting scanning as
573 mutations are $MPA^S$ and/or alter TSS selection (BRABERG *et al.* 2013; YANG *et al.* 2022; BASNET
574 *et al.* 2026). Contemporaneously with our identification of these residues in unbiased genetic
575 selections, P51 mutations were directly tested based on evolutionary analysis of *TFB3*, with P51
576 and R64 conferring strong MPA-sensitivity. Because P51 and R64 substitutions were epistatic
577 with each other, this result was consistent with these residues working together, *e.g.* P51
578 working by enabling positioning of R64 (YANG *et al.* 2024)**.**
579 For TFIIH, physical interactions between Rad3 and Ssl2 may also contribute to TFIIH
580 function in scanning (**Fig. 4j**). Rad3 K499E resulted in suppression of a downstream-shift
581 sensitive reporter and is directly proximal to Ssl2 (**Figs. 2b**, **4j**). We had previously identified
582 mutations in Ssl2 at K357R and K357E (ZHAO *et al.* 2021) near this Rad3 interface sharing the
583 same phenotype as Rad3 K499E, raising the possibility that could be functional interface, with
584 the caveat that Ssl2 K357 may act through other interactions. Because we interpret downstream
585 shifts for Ssl2 mutants as a gain of processivity, there are two possibilities for Rad3 K499E in
586 this framework. First, the interaction between Rad3 and Ssl2 might limit Ssl2 processivity, and
587 therefore we would interpret K499E as a loss of function for the interaction. Alternatively, the
588 interaction between Rad3 and Ssl2 might promote processivity, and K499E confers phenotypes
589 by strengthening the interaction.
590 We further wanted to isolate special "*ssl2*-like" alleles that showed both a $His^+$
591 phenotype on the downstream shift-sensitive *imd2Δ::HIS3* reporter and a $Lys^+$ phenotype due to
592 suppression of the *lys2-128∂* $Spt^-$ phenotype reporter, a phenotype combination exhibited by a

593 specific subset of downstream-shifting *ssl2* mutants (ZHAO *et al.* 2021). These previously
594 identified alleles were highly localized to the DRD domain of Ssl2 (ZHAO *et al.* 2021). Before our
595 Ssl2 work, the Spt$^-$ phenotype had only been observed in conjunction with upstream-shifting
596 phenotypes for alleles of Pol II and the TFIIF subunit Tfg2 (KAPLAN *et al.* 2012; JIN AND KAPLAN
597 2014). Because the Spt$^-$ *ssl2* mutants appeared novel, we wanted to ask if additional GTF
598 mutants with similar phenotypes could be identified, therefore we performed selections with the
599 *imd2Δ::HIS3* reporter selecting on SC-His-Lys medium. While we identified two new alleles of
600 *SSL2*, each with a mutation in Helicase domain 1 (HD1, *ssl2* R378L and *ssl2* W482G), we did
601 not identify additional mutations of this class in other GTFs, suggesting this class of allele may
602 be unique to *SSL2*. Finally, we isolated a TFIIE mutation *tfa1* E374* as a putative downstream
603 shifting allele (**Fig. S2**). Tfa1 has been shown to have inhibitory effect on Tfa2-activated Ssl2
604 translocase activity (LIN AND GRALLA 2005). This suggests *tfa1* E374* could function by relieving
605 restriction on Ssl2 translocase activity, resulting in downstream TSS shift due to increased
606 processivity.
607
608 **Non-PIC mutants conferring suppression of TSS-shift sensitive reporters**
609 Besides PIC factors, our study also isolated non-PIC mutants, comprising putative reporter-
610 specific factors like guanine pathway mutants, indirect effectors like *PMR1*, and
611 chromatin/transcription elongation factors. We found almost fifty percent of initial *IMD2* reporter
612 suppressors had mutations in guanine metabolism genes (**Fig. 5a**). *IMD2* is activated under low
613 GTP conditions, specifically because low GTP induces a TSS switch that bypasses the
614 upstream terminator in the *IMD2* promoter (**Fig. 1a**). Therefore, defects in guanine metabolism
615 create inducing conditions for *IMD2.* We predicted this class of mutant might be differentially
616 sensitive to supplementation by guanine. We found that guanine supplementation suppressed
617 the His$^+$ phenotype of guanine pathway mutants specifically, but not a subset of tested PIC
618 mutants (**Fig. 5a**), and therefore incorporated guanine supplementation into subsequent

619 phenotyping conditions as indicated above. Our WGS also identified an allele of *PMR1* as a
620 suppressor of the *adhΔ50::HIS3* reporter (**Table 1S**). *PMR1* encodes an ER/golgi $Ca^{2+}$/$Mn^{2+}$
621 transporter, and loss of its activity raises cytoplasmic $Mn^{2+}$ levels, conferring $Mn^{2+}$
622 hypersensitivity (RUDOLPH *et al.* 1989; DURR *et al.* 1998; MANDAL *et al.* 2000) (**Fig. 5b**). Our lab
623 had previously found that *pmr1Δ* genetically interacts with increased activity Pol II mutants
624 (BRABERG *et al.* 2013), that increased activity Pol II mutants are specifically sensitive to
625 increased $Mn^{2+}$ (CABART *et al.* 2014), and that *pmr1Δ* itself resulted in an upstream shift to TSS
626 usage at the *ADH1* promoter (QIU *et al.* 2016), due to potential increased Pol II activity in
627 response to heightened cytoplasmic (and nuclear) $Mn^{2+}$ levels. Isolating *pmr1* alleles as
628 suppressors of the *hmo1Δ38::HIS3* reporter would be consistent with potential global effects of
629 $Mn^{2+}$ levels on TSS selection. While $Mn^{2+}$ has many effects on Pol II transcription including
630 perturbing fidelity, it consistently stimulates RNA polymerase catalysis *in vitro e.g.* (NIYOGI *et al.*
631 1981; QIU *et al.* 2024). Therefore, upstream shifts at multiple promoters *in vivo* are consistent
632 with expectations for increased Pol II catalytic activity during initiation caused by increase in
633 cellular $Mn^{2+}$ levels.

634 Intriguingly, we isolated chromatin-related Pol II associated elongation factors as
635 suppressors of both downstream reporters *imd2Δ::HIS3* and *cyc1-1019::HIS3* (**Fig. S3**). Many
636 of these are canonical "Spt" genes and fittingly, some of these were isolated in our double
637 selections for $His^+$ $Lys^+$ ($Spt^-$) suppressors, but a number were isolated from $His^+$ selections. We
638 isolated alleles of *spt2*, *spt5*, *spt16*, *bur2, spn1* and histones from both downstream-sensitive
639 reporters and *spt4* and *spt6* only from the *imd2Δ::HIS3* reporter (**Fig. S3**). This reporter bias
640 may potentially exist because our selections were not saturating. A role for Spt6 in *IMD2* TSS
641 selection has been described for specific *spt6* alleles defective for interaction with a
642 phosphorylated linker in Rpo21/Rpb1 (CONNELL *et al.* 2022). The chromatin/elongation factors
643 we isolated are all known to suppress initiation from cryptic promoters within genes (WINSTON *et*
644 *al.* 1984; CLARK-ADAMS *et al.* 1988; KAPLAN *et al.* 2003; CHEUNG *et al.* 2008; DORIS *et al.* 2018).

645 Similarly, their Spt$^-$ phenotypes at *lys2-128∂* are consistent with a chromatinized-promoter within
646 a transcription unit (in this case, a Ty1 *∂* element within the *LYS2* gene) being activated upon
647 elongation-mediated chromatin disruption in specific mutants (SIMCHEN *et al.* 1984; WINSTON *et*
648 *al.* 1984; CLARK-ADAMS *et al.* 1988; SWANSON *et al.* 1991; PRELICH AND WINSTON 1993;
649 FISCHBECK *et al.* 2002; KAPLAN *et al.* 2003; CHEUNG *et al.* 2008; CUI *et al.* 2016; DORIS *et al.*
650 2018). This would be a reasonable model to explain suppression of *imd2Δ::HIS3* because the
651 *IMD2* promoter (driving His$^+$) is transcribed as part of an upstream CUT transcript (KOPCEWICZ
652 *et al.* 2007; JENKS *et al.* 2008; KUEHNER AND BROW 2008), potentially sensitizing the
653 downstream TSS to chromatin defects driven by Pol II elongation. Conversely, this model does
654 not easily explain why we also identified chromatin/elongation gene alleles as suppressors of
655 *cyc1-1019::HIS3* (see Discussion) and raises the possibility that chromatin factors might globally
656 alter TSS selection, which we test directly below.
657
658 **Functional characterization of TSS mutants through genetic interaction analyses**
659 After our genetic selections, we wanted to functionally characterize mutants using genetic
660 interactions. In our prior studies, both additive/synergistic and epistatic interactions have been
661 observed for TSS-shifting mutants leading to a framework where mutants are interpreted as
662 affecting initiation efficiency (i.e. Pol II catalysis) or scanning processivity (TFIIH/PIC functions).
663 Previous examination of double mutants between Pol II catalytic mutants and TFIIB or TFIIF
664 alleles showed additivity across combinations (enhancement when mutants shift TSSs the same
665 direction and suppression when they shift in opposite directions). However, in other
666 combinations, we observed epistasis where double mutants exhibited the TSS phenotype of
667 one of the single mutants and not the other. This was especially clear when upstream shifting
668 Pol II mutants were combined with downstream shifting *ssl2* alleles, leading to the hypothesis
669 that the tested *ssl2* alleles increased scanning processivity, but this didn't lead to downstream
670 TSS shifts in mutants that increased initiation upstream. Regardless of mechanistic models for

671 how mutants are genetically interacting, double mutant analysis can reveal when mutations are
672 dependent on one another (epistasis), which is indicative of their defects being at the same
673 step, or when mutations function redundantly in an essential step (synergy or synthetic lethality),
674 or when mutations are perturbing a system independently, whereby double mutant phenotypes
675 will be the additive consequences of the single mutants combined. To therefore functionally
676 dissect our mutants, we tested interactions at inter-subunit interfaces and further analyzed
677 functional interactions across the PIC (**Figs. 6b, 6c; 7; S4**).
678 We first tested a potential Rpb10-Tfg1 interface in TSS selection by genetic interaction
679 studies and site-directed mutagenesis. We isolated *rpb10* L25S as a downstream-shifting
680 suppressor of the *imd2Δ::HIS3* reporter and showed this allele could also suppress the *cyc1-*
681 *1019::HIS3* reporter (**Fig. 2b**). Because Rpb10 is a common subunit shared amongst three RNA
682 polymerases, it was interesting to find a Pol II-specific phenotype. Examination of Pol PIC
683 structures for Pol I, II, and III PICs suggested that an interaction between Rpb10 in the vicinity of
684 the Rpb10 helix-loop-helix L25 residue might only be present in the Pol II PIC, where Rpb10
685 appears to contact a loop in the Tfg1 N-terminal domain (**Fig. 6b**). This potential interaction
686 suggested that Rpb10 might affect Pol II TSS distributions through an interaction with TFIIF
687 subunit Tfg1 that may be perturbed in the *rpb10* L25S allele. To examine this, we targeted
688 Rpb10 E29 and Tfg2 R26 residues that display potential interactions based on structural studies
689 (SCHILBACH *et al.* 2021) (**Fig. 6c**). We generated a series of genomic mutations by CRISPR
690 including charge reversals at both residues and assessed growth and TSS-shift reporter
691 phenotypes. On analysis of mutants, we did not observe overall growth defects in *tfg*1 single or
692 *tfg1 rpb10* double mutants (**Fig. 6c**, rows 6 and 7). Charge reversal *rpb10* mutation of E29R
693 resulted in suppression of the downstream shift reporter while E29A did not display effects (**Fig.**
694 **6c**, rows 3 and 4). However, when *rpb10* E29R was combined with the *tfg1* R26A or R26E
695 mutations, apparent suppression of the downstream shift phenotype was observed (**Fig. 6c**,
696 rows 10 and 11). Moreover, we found that *tfg1* mutants also suppressed the leaky $His^+$

697 phenotype of *imd2Δ::HIS3*, with Tfg1 R26E being more robust than R26A (**Fig. 6c**, rows 6 and
698 7, SC-His panel). Suppression of the leaky His$^+$ phenotype of *imd2Δ::HIS3* might result from an
699 upstream TSS-shifting phenotype, therefore we tested these *tfg1* mutants against the upstream
700 reporter *adhΔ50::HIS3* (**Fig. 6c**, lower panel) but *tfg1* mutants did not suppress *adhΔ50::HIS3*.
701 These results show that an additional *rpb10* allele can alter TSS selection (**Fig. 6c**) and that its
702 phenotype can be modulated by proximal *tfg1* alleles. However, we could not prove that Rpb10-
703 Tfg1 interactions underlie the *rpb10* L25S mutant phenotype.
704 We tested additional functional interactions by tetrad dissection analysis of diploids
705 followed by fitness analysis of each spore by pixel quantification using EBImage (PAU *et al.*
706 2010; NAMJILSUREN AND ARNDT 2025). We then calculated "expected" double mutant growth
707 phenotype from single mutant phenotypes by a multiplicative model for independent effects on
708 fitness of single mutants in a double mutant combination (MANI *et al.* 2008) and compared this
709 expected double mutant growth phenotype to the observed double mutant growth phenotype.
710 Genetic interactions were established based on comparisons of these double mutant metrics.
711 We examined upstream shifting *rpb9Δ* genetic interactions with a panel of mutants. First, we
712 examined *rpb9Δ* in conjunction with the upstream-shifting *rpb2* G369C as the proximity of Rpb9
713 to Rpb2 and TFIIF raises the possibility that these mutants work in the same pathway, as it has
714 previously been proposed that *rpb2 G369C* works through effects on TFIIF. Second, we tested
715 *rpb9Δ* against a subset of our novel downstream shifting alleles to ask if they were additive or
716 epistatic. The GTF TFIIF binds at the interface between Rpb9 and Rpb2 in the protrusion-lobe
717 domain with proximity to Rpb2 G369 (**Fig. 4, 7b**)(CHEN *et al.* 2007). Because *rpb2* G369C and
718 *rpb9Δ* are both upstream shifting mutations, it is expected that the double mutant in case of non-
719 interaction would be a product of individual fitnesses. Conversely, if they functioned together in
720 the same process, we might observe less than multiplicative effects (sometimes referred to as a
721 specific form of epistasis). Instead, we observed growth fitness of *rpb2* G369C *rpb9Δ* double

722 mutants to be worse than predicted from the multiplicative model, indicating a synthetic defect
723 (**Fig. 7d**).
724 When combining upstream shifting *rpb9*Δ with a panel of downstream shifting mutants,
725 *tfb2* F189S, *tfb4* N71K, *ssl1* I122T, *rad3* K499E, *rpb10* L25S and *tfg2* C222Y by tetrad
726 dissection analysis (**Fig. S4**). We found *rpb9*Δ *rpb10* L25S double mutant fitness to be similar to
727 the *rpb9*Δ single mutant growth defect, with resultant fitness around the predicted fitness (**Fig.**
728 **S4**, bottom, middle). In addition, we found *rpb9Δ tfg2* C222Y double mutant fitness to be slightly
729 worse than expected (**Fig. S4**, bottom, right). Because these mutants have opposite effects on
730 TSS shifts, combination might be predicted to result in suppression of growth defects, if the
731 effects of each mutant on TSS selection are additive *and* the growth defects observed
732 correspond to the TSS selection phenotype. This kind of interaction between *rpb9*Δ and *rpb10*
733 L25S to be epistatic where the defect of one mutation (upstream) cannot be compensated by a
734 second mutation working in an opposite direction (downstream). Conversely, for interaction
735 between *tfg2* C22Y and *rpb9*Δ, if either of the *tfg2* C222Y or *rpb9*Δ effects required a WT allele
736 for their specific phenotypes, then instead of suppression of phenotypes by two opposite acting
737 alleles, we might observe exacerbation due to conversion of a downstream or upstream shifting
738 allele to the other class in the double mutant. Assuming the change in growth fitness reflects an
739 equivalent change in TSS selection, this kind of interaction could represent sign epistasis.
740 In contrast to the *rpb9*Δ-*tfg2* C222Y negative interaction, we observed clear double mutant
741 suppression between *rpb9*Δ *tfb2* F189S, *rpb9*Δ *tfb4* N71K, *rpb9*Δ *ssl1* I122T and *rpb9Δ rad3*
742 K499E, where each TFIIH allele suppressed growth defects associated with *rpb9*Δ (**Fig. S4**, top
743 panel and bottom, left). This indicates that the growth defect induced by upstream mutant *rpb9Δ*
744 was compensated by all tested TFIIH downstream mutants and suggesting that the growth
745 defect of *rpb9*Δ could be initiation related. This supposition is because TFIIH's gene expression
746 functions are limited to the PIC. This result was unexpected based on a simple model where the
747 *rpb9*Δ upstream-shifting phenotype would be caused by loss of its restraint of the key Pol II

748 catalytic domain, the trigger loop (TL) (KASTER *et al.* 2016). This model was based on *rpb9*Δ
749 conferring similar phenotypes to hyperactive mutants in the Rpb1 TL (upstream TSS shifts and
750 increased elongation rate *in vitro*). Upstream-shifting TL mutants are epistatic to downstream-
751 shifting *ssl2* TFIIH alleles, and therefore similar interactions between *rpb9*Δ and downstream-
752 shift reporter specific-TFIIH alleles was what was previously expected (see Discussion).
753
754 **Novel PIC alleles shift TSSs genome wide while chromatin/elongation alleles have muted**
755 **effects**
756 To gain insight into the function of a subset of our TSS shifting mutants, we quantified TSSs
757 across a curated set of promoters genome wide by STRIPE-seq in WT and mutant strains
758 (POLICASTRO *et al.* 2020; POLICASTRO *et al.* 2021; POLICASTRO AND ZENTNER 2022) (**Fig. 8a**).
759 We chose 8 downstream-shifting mutants, six from the PIC class and two from the
760 chromatin/elongation class isolated in our studies namely *tfb4* N71K, *rad3* K499E, *ssl1* I122T,
761 *tfb2* F189S, *rpb1* A480S, and *rpb1*0 L25S (PIC mutants) and *spn1* V199G and *spt5* G814*
762 (chromatin/elongation mutants) together with their corresponding WT parents (**Figs. 8**, **9**, **S5**,
763 **S6**). To assess TSS shifts in mutants relative to WT parents, we quantified TSSs as in our
764 previous studies (QIU *et al.* 2020; ZHAO *et al.* 2021) along with STRIPE-seq processing as in
765 (POLICASTRO *et al.* 2021). We focused our TSS analyses to 5979 Pol II promoter regions (RHEE
766 AND PUGH 2012; QIU *et al.* 2020; ZHAO *et al.* 2021) filtered to include promoters passing a cutoff
767 of a read count threshold in the promoter window analyzed resulting in analysis of n=2829
768 promoters. TSS usage values were then compared to those in WT by two TSS shift metrics as
769 in (QIU *et al.* 2020; ZHAO *et al.* 2021): shift in median TSS (Δmedian), which represents the
770 difference in median position of the TSS distribution at a promoter between a mutant and WT
771 strains (**Fig. 8b**) and change in spread (Δspread) that represents the change in width of
772 promoter TSS distributions relative to WT (**Fig. 9a**).

773 Individual replicates were generally reproducible for Δmedian TSS (**Fig. S5**). Principal
774 component analysis (PCA) of the Δmedian values of combined replicates showed three clusters
775 representing functional differences across the primary axis of variance (**Fig. 8c**): cluster 1
776 contained *rpb1* A480S, *rpb10* L25S, *ssl1* I122T and *tfb4* N71K, cluster 2 contained *rad3* K499E
777 and *tfb2* F189S, and cluster 3 contained *spt5* G814* and *spn1* V199G. When examining PCA of
778 individual replicates each compared to the average WT median position (**Fig. S5b**)**,** we found
779 chromatin alleles to cluster near the WT, suggesting they only have mild effects on TSS
780 distributions globally, but with greater effects for *spt5* G814* than for *spn1* V199G (**Fig. 8f**).
781 While both chromatin/elongation alleles did have effects beyond just an individual reporter, their
782 effects were quantitatively and qualitatively different from PIC alleles, consistent with potentially
783 relating to the chromatin context of individual promoters rather than innately affecting TSS
784 selection and promoter scanning at all promoters. All PIC alleles showed a large bias towards
785 downstream shifts in TSS distribution across the majority of promoters, with *rad3* K499E and
786 *tfb2* F189S showing the strongest effects (**Fig. 8f**).
787 PCA of Δspread values also displayed three groups and examination of PCA for
788 individual replicates of all strains compared to the average WT behavior shows that
789 chromatin/elongation mutants cluster with WT, most PIC mutants cluster together while *rad3*
790 K499E and *tfb2* F189S, which showed the strongest effects on Δmedian TSS, formed a
791 separate cluster based on Δspread (**Figs. 9, S6**). Examination of directional bias in spread
792 suggests that while spread was perturbed for most mutants, *rad3* K499E and *tfb2* F189S
793 showed the strongest increase in spread, consistent with the downstream shift in TSS usage
794 also expanding TSS spread to downstream positions (**Figs. 9e, S6d**). These results again
795 differentiated two TFIIH alleles, *rad3* K499E and *tfb2* F189S, from two others, *ssl1* I122T and
796 *tfb4* N71K.
797

798 **DISCUSSION**

799 Our studies reveal the wider landscape of genes and specific mutations that can alter the TSS
800 selection in yeast. In addition to independently identifying some already discovered alleles,
801 validating our novel reporters, we also identified an array of novel alleles suppressing our
802 initiation reporters. Notably, we did not find additional factors associated with promoters but not
803 directly connected to the PIC, such as chromatin remodelers or transcription coactivators, as
804 able to suppress our initiation reporters. This could simply be due to these remodelers not
805 strongly functioning in TSS accessibility at our reporters, or at least not in a way that might allow
806 reporter suppression upon their mutation. We find that mutations in many PIC components
807 including Rpb10 and additional TFIIH subunits can perturb initiation by promoter scanning when
808 mutated. Importantly, we find that the novel *rpb10* allele and tested TFIIH alleles alter TSS
809 selection genome wide. Our prior studies, new alleles identified here, and our parallel studies on
810 the Pol II/PIC interface reinforce that upstream shifting of TSSs results from compromise of
811 TFIIH-PIC interactions through the Tfb3-TFIIE-Rpb7 interface (BRABERG *et al.* 2013; YANG *et al.*
812 2022; YANG *et al.* 2024; BASNET *et al.* 2026). We extend evidence that the Rpb2-TFIIB
813 interaction is important for promoter scanning while also finding that perturbation to Rpo21/Rpb1
814 and Rpb2 broadly leads to suppression of downstream-shift sensitive reporters. This latter result
815 further supports the idea that defective Pol II catalysis/initiation activity results in phenotypes
816 consistent with downstream shifts in TSS usage. In contrast, we also have identified novel TFIIH
817 downstream-shifting alleles that are generally not located at inter-subunit interfaces, save one.

818 The downstream-shifting phenotype of these novel TFIIH alleles would be consistent
819 with a gain of function in TFIIH scanning processivity or rate. One interpretation of our alleles in
820 Rad3, Tfb2, Tfb4, and Ssl1 based on their locations is that they alter plasticity or dynamics
821 within the TFIIH structure. When this plasticity is altered, perturbations may propagate either to
822 the Ssl2 active site or to Ssl2 DNA binding properties, which in turn allow scanning to be
823 extended to downstream positions through increased processivity or increased scanning rate.

824 The idea that TFIIH processivity can be sensitive to small structural perturbations provides a
825 conceivable evolutionary path for TFIIH to gain ability to reach downstream TSSs during the
826 advent of the promoter scanning mechanism.

827 Potential communication between Ssl2 and the rest of the PIC can take a few paths.
828 First, there is a connection from Ssl2 to Tfb3 and Pol II/TFIIE through the following proteins:
829 Ssl2 to Tfb2 to Tfb4 to Ssl1 to Rad3 to Tfb3. Second, Tfb1 drapes over multiple TFIIH
830 components and connects to Tfa1 from TFIIE. Finally, Rad3 has a small number of residues
831 that may close the gap between it and Ssl2 and contact Ssl2 residues. We have identified
832 alleles along components that form the path from Ssl2 to Tfb3 (Tfb2, Tfb4, Ssl1, Tfb3) and
833 between Rad3 and Ssl2. If the protein connection between Ssl2 to Tfb3 has a certain amount of
834 flexibility or dynamics (using an analogy of an accordion's bellows or a pantograph that might
835 tolerate or allow extension or contraction, depending on rigidity), then alterations to this flexibility
836 might have consequences for Ssl2 rate or processivity as it translocates downstream on
837 promoter DNA. The locations of putative gain of function Tfb2, Tfb4, and Ssl1 alleles are all
838 consistent with perturbing internal intra-subunit interactions and we would propose they
839 increase flexibility of the "bellows" or "pantograph" formed by these components that connect
840 Ssl2 to Tfb3 and the PIC. This increased flexibility may then allow Ssl2 to translocate longer or
841 faster, resulting in a shift in TSS usage to downstream positions. Future biochemical and
842 biophysical experiments, potentially coupled with molecular dynamics simulations, might provide
843 tests of a model that, first, novel TFIIH alleles do indeed confer increased TFIIH processivity,
844 and second, that these alleles might alter structural properties of TFIIH in similar ways.

845 Chromatin/elongation factors can be envisioned to function in controlling initiation in two
846 ways. First, native chromatin architecture may reduce transcription initiation from nucleosome-
847 occluded TSSs (most yeast promoters have TSSs located within the boundaries of +1
848 nucleosomes) (RANDO AND WINSTON 2012). If there are downstream shifts in nucleosomes
849 dependent on elongation factors, then this could feed back to TSS usage and relax nucleosomal

850 inhibition of nucleosome-sensitive TSSs for promoters with appropriately positioned +1
851 nucleosomes. Second, if a promoter's TSSs are transcribed themselves from an upstream
852 promoter, then promoter-associated nucleosomes that are transcribed dependent on an
853 upstream TSS could become dependent on factors that restore transcribed nucleosomes in the
854 wake of elongating Pol II. This situation might reflect allele-selective effects on TSS usage for
855 transcribed promoters and less so global effects. This arrangement of an upstream promoter
856 driving transcription of a downstream promoter and thereby sensitizing the chromatin over the
857 downstream promoter is similar to that observed at the *SRG1-SER3* locus (MARTENS *et al.*
858 2004) and also the structure of the *lys2-128∂* allele (SIMCHEN *et al.* 1984). Each of these loci are
859 especially sensitive to chromatin and transcription elongation defects, and the latter of which
860 was used in the original identification of a number of the Spt chromatin/elongation factors –
861 factors that we isolated with our reporters here (SIMCHEN *et al.* 1984; CLARK-ADAMS AND
862 WINSTON 1987; CLARK-ADAMS *et al.* 1988; MALONE *et al.* 1991; SWANSON *et al.* 1991; CUI *et al.*
863 2016). In these cases, chromatin maintenance suppresses transcription initiation from within the
864 transcribed regions. Altered chromatin architecture in chromatin mutants can result in
865 widespread initiation from cryptic promoters (PRELICH AND WINSTON 1993; KAPLAN *et al.* 2003;
866 CHU *et al.* 2007; CHEUNG *et al.* 2008; DORIS *et al.* 2018) but perhaps also from chromatin-
867 sensitive TSSs adjacent to existing promoters. In either case, altered chromatin can result in
868 increased transcription from "suppressed" sites.
869 We rationalize the identification of chromatin elongation factors from the *imd2Δ::HIS3*
870 reporter because of its idiosyncratic transcription from upstream TSSs (generating a cryptic
871 unstable transcript (CUT) (DAVIS AND ARES 2006; KOPCEWICZ *et al.* 2007; JENKS *et al.* 2008;
872 KUEHNER AND BROW 2008)) that likely contributes to or controls nucleosome positioning over the
873 downstream, low-guanine inducible TSS. It was already known that certain *spt6* alleles could
874 increase usage of downstream TSSs at *IMD2* in the absence of known inducing conditions
875 (CONNELL *et al.* 2022). Here, we extend identification of chromatin and elongation factors that

876 can act at *IMD2* through suppression of *imd2Δ::HIS3* to *spt2*, *spt4*, *spt5*, *spt16*, *spn1*, *bur2, hta1,*
877 and *htb1* alleles. These results suggest that *imd2Δ::HIS3* may be similarly sensitive to the
878 chromatin/Spt$^-$ class of mutant as is the classical *lys2-128∂* allele. However, we also isolated
879 chromatin mutants suppressing *cyc1-1019::HIS3* in addition to *imd2Δ::HIS3.* This *cyc1* allele
880 was inserted into a non-native locus that is devoid of genes that has previously been used to
881 house reporter genes (GRUBER *et al.* 2012). Our initial presumption was that the *CYC1* promoter
882 would not be itself transcribed, but examination of data from the Steinmetz lab (XU *et al.* 2009)
883 suggests that our *CYC1* promoter fragment also contains *SUT215*, a stable unannotated
884 transcript, and that integration of *cyc1-1019::HIS3* at chrI:199270-199271 causes it to be
885 flanked by *SUT004* upstream and *CUT442* downstream. Taken together, these provide support
886 that *cyc1-1019::HIS3* sensitivity to chromatin and elongation factors could be through
887 transcription over its promoter altering promoter nucleosomes, and we speculate
888 chromatin/elongation effects at other promoters may relate especially to those promoters that
889 have overlapping transcription units.
890
891 **Limitations of the study**
892 Our genetic interaction analysis indicated some interesting relationships between reporter
893 suppressor alleles, specifically the suppression observed between a subset of downstream-
894 shifting TFIIH alleles and *rpb9Δ*. Our previous genetic interaction studies showed that upstream
895 shifting Pol II catalytic alleles were epistatic to downstream-shifting *ssl2* alleles for both growth
896 phenotypes and for TSS shifts at *ADH1* (ZHAO *et al.* 2021). Our previous understanding for
897 *rpb9Δ* was that it was functioning similarly to upstream-shifting Pol II catalytic alleles (KASTER *et*
898 *al.* 2016). This assumption, coupled with the assumption that novel downstream-shifting TFIIH
899 alleles should function like *ssl2* downstream-shifting alleles, led to the expectation that *rpb9Δ*
900 would be epistatic to TFIIH alleles for TSS shift phenotypes. Additionally, we had the
901 expectation that *rpb9Δ* growth phenotypes related to its elongation defects and would not

902 necessarily be suppressible by initiation factor mutants. Contrary to these expectations, we find
903 the possibility of complexity in genetic interactions that might indicate different initiation alleles
904 are working in more complex ways than we had previously thought. We imagine these results
905 should be developed and extended in a few ways. For example, double mutant combinations of
906 *rpb9*Δ and existing *ssl2* alleles and of Pol II alleles with novel TFIIH alleles would also allow
907 understanding of potential allele specificity. Additionally, examination of double mutants for
908 phenotypes on transcription reporters would allow to assess if initiation specific phenotypes
909 reflect overall growth phenotypes. Finally, quantitative primer extension analysis of double
910 mutants for *ADH1* TSS selection would also determine if growth phenotypes correlate with
911 specific changes to TSS distributions at promoters, where *ADH1* promoter has extensively
912 served as an excellent target for TSS distribution change assessment.
913
914 **Data availability**
915 Sequencing data generated in this study are available in the NCBI BioProject under accession
916 number PRJNA1337182. Strains used in this study, outlined in **Tables S1** and **S2**, are available
917 from the corresponding author upon request.
918
919 **Acknowledgements**
920 We acknowledge Dr. David Brow at the University of Wisconsin for guidance on genetic
921 selections. We are especially grateful to the students of BIOSC 0068 Foundations of Biology
922 Laboratory 2 course at the University of Pittsburgh for genetic selection of candidates leading to
923 identification of a subset of alleles described here. We acknowledge Gabe Zentner, Robert
924 Policastro, and Chhabi Govind for advice on STRIPE-seq. We would like to dedicate this paper
925 to the memory of Gabe Zentner.
926

**Funding**

Supported by funding from National Institutes of Health grants R01GM120450 and R35GM144116 to C.D.K. This research was supported in part by the University of Pittsburgh Center for Research Computing and Data, RRID:SCR_022735, through the resources provided. Specifically, this work used the HTC cluster, which is supported by NIH award number S10OD028483.

**Conflict of interest**

The authors declare no conflicts of interest.

936 **REFERENCES**


937 Picard Toolkit 2019. Broad Institute, Broad Institute, GitHub Repository.
938 https://broadinstitute.github.io/picard/.
939 Aibara, S., S. Schilbach and P. Cramer, 2021 Structures of mammalian RNA polymerase II pre-
940 initiation complexes. Nature 594**:** 124-128.
941 Amberg, D. C., D. J. Burke and J. N. Strathern, 2005 Methods in Yeast Genetics: A Cold Spring
942 Harbor Laboratory Course Manual. Cold Spring Harbor, NY: Cold Spring Harbor
943 PressCold Spring Harbor, NY: Cold Spring Harbor Press.
944 Arribere, J. A., and W. V. Gilbert, 2013 Roles for transcript leaders in translation and mRNA
945 decay revealed by transcript leader sequencing. Genome Res 23**:** 977-987.
946 Baek, I., L. J. Friedman, J. Gelles and S. Buratowski, 2021 Single-molecule studies reveal
947 branched pathways for activator-dependent assembly of RNA polymerase II pre-initiation
948 complexes. Mol Cell 81**:** 3576-3588 e3576.
949 Bangur, C. S., T. S. Pardee and A. S. Ponticelli, 1997 Mutational analysis of the D1/E1 core
950 helices and the conserved N-terminal region of yeast transcription factor IIB (TFIIB):
951 identification of an N-terminal mutant that stabilizes TATA-binding protein-TFIIB-DNA
952 complexes. Mol Cell Biol 17**:** 6784-6793.
953 Basnet, P., Y. Zhu, I. O. Vvedenskaya, P. Arora, S. Hammer *et al.*, 2026 Important role in
954 transcription start site selection for the RNA polymerase II-TFIIE-TFIIH interface in
955 Saccharomyces cerevisiae. Genetics.
956 Berroteran, R. W., D. E. Ware and M. Hampsey, 1994 The sua8 suppressors of Saccharomyces
957 cerevisiae encode replacements of conserved residues within the largest subunit of RNA
958 polymerase II and affect transcription start site selection similarly to sua7 (TFIIB)
959 mutations. Mol Cell Biol 14**:** 226-237.
960 Bolger, A. M., M. Lohse and B. Usadel, 2014 Trimmomatic: a flexible trimmer for Illumina
961 sequence data. Bioinformatics 30**:** 2114-2120.
962 Braberg, H., H. Jin, E. A. Moehle, Y. A. Chan, S. Wang *et al.*, 2013 From structure to systems:
963 high-resolution, quantitative genetic analysis of RNA polymerase II. Cell 154**:** 775-788.
964 Breathnach, R., and P. Chambon, 1981 Organization and expression of eucaryotic split genes
965 coding for proteins. Annu Rev Biochem 50**:** 349-383.
966 Brow, D. A., 2019 An Allosteric Network for Spliceosome Activation Revealed by High-
967 Throughput Suppressor Analysis in Saccharomyces cerevisiae. Genetics 212**:** 111-124.
968 Buratowski, S., S. Hahn, P. A. Sharp and L. Guarente, 1988 Function of a yeast TATA element-
969 binding protein in a mammalian transcription system. Nature 334**:** 37-42.
970 Cabart, P., H. Jin, L. Li and C. D. Kaplan, 2014 Activation and reactivation of the RNA
971 polymerase II trigger loop for intrinsic RNA cleavage and catalysis. Transcription 5**:**
972 e28869.
973 Chen, B. S., and M. Hampsey, 2004 Functional interaction between TFIIB and the Rpb2 subunit
974 of RNA polymerase II: implications for the mechanism of transcription initiation. Mol Cell
975 Biol 24**:** 3983-3991.
976 Chen, H. T., L. Warfield and S. Hahn, 2007 The positions of TFIIF and TFIIE in the RNA
977 polymerase II transcription preinitiation complex. Nat Struct Mol Biol 14**:** 696-703.
978 Cheung, V., G. Chua, N. N. Batada, C. R. Landry, S. W. Michnick *et al.*, 2008 Chromatin- and
979 transcription-related factors repress transcription from within coding regions throughout
980 the Saccharomyces cerevisiae genome. PLoS Biol 6**:** e277.
981 Chu, Y., R. Simic, M. H. Warner, K. M. Arndt and G. Prelich, 2007 Regulation of histone
982 modification and cryptic transcription by the Bur1 and Paf1 complexes. EMBO J 26**:**
983 4646-4656.

Cingolani, P., A. Platts, L. Wang le, M. Coon, T. Nguyen *et al.*, 2012 A program for annotating and predicting the effects of single nucleotide polymorphisms, SnpEff: SNPs in the genome of Drosophila melanogaster strain w1118; iso-2; iso-3. Fly (Austin) 6**:** 80-92.

Clark-Adams, C. D., D. Norris, M. A. Osley, J. S. Fassler and F. Winston, 1988 Changes in histone gene dosage alter transcription in yeast. Genes Dev 2**:** 150-159.

Clark-Adams, C. D., and F. Winston, 1987 The SPT6 gene is essential for growth and is required for delta-mediated transcription in Saccharomyces cerevisiae. Mol Cell Biol 7**:** 679-686.

Coin, F., J. C. Marinoni, C. Rodolfo, S. Fribourg, A. M. Pedrini *et al.*, 1998 Mutations in the XPD helicase gene result in XP and TTD phenotypes, preventing interaction between XPD and the p44 subunit of TFIIH. Nat Genet 20**:** 184-188.

Conaway, R. C., and J. W. Conaway, 1993 General initiation factors for RNA polymerase II. Annu Rev Biochem 62**:** 161-190.

Connell, Z., T. J. Parnell, L. L. McCullough, C. P. Hill and T. Formosa, 2022 The interaction between the Spt6-tSH2 domain and Rpb1 affects multiple functions of RNA Polymerase II. Nucleic Acids Res 50**:** 784-802.

Cramer, P., D. A. Bushnell and R. D. Kornberg, 2001 Structural basis of transcription: RNA polymerase II at 2.8 angstrom resolution. Science 292**:** 1863-1876.

Cui, P., H. Jin, M. R. Vutukuru and C. D. Kaplan, 2016 Relationships Between RNA Polymerase II Activity and Spt Elongation Factors to Spt- Phenotype and Growth in Saccharomyces cerevisiae. G3 (Bethesda) 6**:** 2489-2504.

Danecek, P., A. Auton, G. Abecasis, C. A. Albers, E. Banks *et al.*, 2011 The variant call format and VCFtools. Bioinformatics 27**:** 2156-2158.

Danecek, P., J. K. Bonfield, J. Liddle, J. Marshall, V. Ohan *et al.*, 2021 Twelve years of SAMtools and BCFtools. Gigascience 10.

Davis, C. A., and M. Ares, Jr., 2006 Accumulation of unstable promoter-associated transcripts upon loss of the nuclear exosome subunit Rrp6p in Saccharomyces cerevisiae. Proc Natl Acad Sci U S A 103**:** 3262-3267.

Deatherage, D. E., and J. E. Barrick, 2014 Identification of mutations in laboratory-evolved microbes from next-generation sequencing data using breseq. Methods Mol Biol 1151**:** 165-188.

Dobin, A., C. A. Davis, F. Schlesinger, J. Drenkow, C. Zaleski *et al.*, 2013 STAR: ultrafast universal RNA-seq aligner. Bioinformatics 29**:** 15-21.

Doris, S. M., J. Chuang, O. Viktorovskaya, M. Murawska, D. Spatt *et al.*, 2018 Spt6 Is Required for the Fidelity of Promoter Selection. Mol Cell 72**:** 687-699 e686.

Dudnyk, K., D. Cai, C. Shi, J. Xu and J. Zhou, 2024 Sequence basis of transcription initiation in the human genome. Science 384**:** eadj0116.

Durr, G., J. Strayle, R. Plemper, S. Elbs, S. K. Klee *et al.*, 1998 The medial-Golgi ion pump Pmr1 supplies the yeast secretory pathway with Ca2+ and Mn2+ required for glycosylation, sorting, and endoplasmic reticulum-associated protein degradation. Mol Biol Cell 9**:** 1149-1162.

Eichner, J., H. T. Chen, L. Warfield and S. Hahn, 2010 Position of the general transcription factor TFIIF within the RNA polymerase II transcription preinitiation complex. EMBO J 29**:** 706-716.

Ellison, M. A., J. L. Walker, P. J. Ropp, J. D. Durrant and K. M. Arndt, 2020 MutantHuntWGS: A Pipeline for Identifying Saccharomyces cerevisiae Mutations. G3 (Bethesda) 10**:** 3009-3014.

Faitar, S. L., S. A. Brodie and A. S. Ponticelli, 2001 Promoter-specific shifts in transcription initiation conferred by yeast TFIIB mutations are determined by the sequence in the immediate vicinity of the start sites. Mol Cell Biol 21**:** 4427-4440.

1034 Fazal, F. M., C. A. Meng, K. Murakami, R. D. Kornberg and S. M. Block, 2015 Real-time
1035 observation of the initiation of RNA polymerase II transcription. Nature 525: 274-277.
1036 Fischbeck, J. A., S. M. Kraemer and L. A. Stargell, 2002 SPN1, a conserved gene identified by
1037 suppression of a postrecruitment-defective yeast TATA-binding protein mutant. Genetics
1038 162: 1605-1616.
1039 Fishburn, J., E. Tomko, E. Galburt and S. Hahn, 2015 Double-stranded DNA translocase activity
1040 of transcription factor TFIIH and the mechanism of RNA polymerase II open complex
1041 formation. Proc Natl Acad Sci U S A 112: 3961-3966.
1042 Freire-Picos, M. A., S. Krishnamurthy, Z. W. Sun and M. Hampsey, 2005 Evidence that the
1043 Tfg1/Tfg2 dimer interface of TFIIF lies near the active center of the RNA polymerase II
1044 initiation complex. Nucleic Acids Res 33: 5045-5052.
1045 Furter-Graves, E. M., R. Furter and B. D. Hall, 1991 SHI, a new yeast gene affecting the
1046 spacing between TATA and transcription initiation sites. Mol Cell Biol 11: 4121-4127.
1047 Furter-Graves, E. M., and B. D. Hall, 1990 DNA sequence elements required for transcription
1048 initiation of the Schizosaccharomyces pombe ADH gene in Saccharomyces cerevisiae.
1049 Mol Gen Genet 223: 407-416.
1050 Ghazy, M. A., S. A. Brodie, M. L. Ammerman, L. M. Ziegler and A. S. Ponticelli, 2004 Amino
1051 acid substitutions in yeast TFIIF confer upstream shifts in transcription initiation and
1052 altered interaction with RNA polymerase II. Mol Cell Biol 24: 10975-10985.
1053 Giardina, C., and J. T. Lis, 1993 DNA melting on yeast RNA polymerase II promoters. Science
1054 261: 759-762.
1055 Greger, I. H., A. Aranda and N. Proudfoot, 2000 Balancing transcriptional interference and
1056 initiation on the GAL7 promoter of Saccharomyces cerevisiae. Proc Natl Acad Sci U S A
1057 97: 8415-8420.
1058 Greger, I. H., and N. J. Proudfoot, 1998 Poly(A) signals control both transcriptional termination
1059 and initiation between the tandem GAL10 and GAL7 genes of Saccharomyces
1060 cerevisiae. EMBO J 17: 4771-4779.
1061 Gruber, J. D., K. Vogel, G. Kalay and P. J. Wittkopp, 2012 Contrasting properties of gene-
1062 specific regulatory, coding, and copy number mutations in Saccharomyces cerevisiae:
1063 frequency, effects, and dominance. PLoS Genet 8: e1002497.
1064 Hampsey, M., 1991 A tester system for detecting each of the six base-pair substitutions in
1065 Saccharomyces cerevisiae by selecting for an essential cysteine in iso-1-cytochrome c.
1066 Genetics 128: 59-67.
1067 Hampsey, M., 2006 The Pol II initiation complex: finding a place to start. Nat Struct Mol Biol 13:
1068 564-566.
1069 He, Y., C. Yan, J. Fang, C. Inouye, R. Tjian *et al.*, 2016 Near-atomic resolution visualization of
1070 human transcription promoter opening. Nature 533: 359-365.
1071 Hekmatpanah, D. S., and R. A. Young, 1991 Mutations in a conserved region of RNA
1072 polymerase II influence the accuracy of mRNA start site selection. Mol Cell Biol 11:
1073 5781-5791.
1074 Hemming, S. A., D. B. Jansma, P. F. Macgregor, A. Goryachev, J. D. Friesen *et al.*, 2000 RNA
1075 polymerase II subunit Rpb9 regulates transcription elongation in vivo. J Biol Chem 275:
1076 35506-35511.
1077 Hull, M. W., K. McKune and N. A. Woychik, 1995 RNA polymerase II subunit RPB9 is required
1078 for accurate start site selection. Genes Dev 9: 481-490.
1079 Hurowitz, E. H., and P. O. Brown, 2003 Genome-wide analysis of mRNA lengths in
1080 Saccharomyces cerevisiae. Genome Biol 5: R2.
1081 Janke, C., M. M. Magiera, N. Rathfelder, C. Taxis, S. Reber *et al.*, 2004 A versatile toolbox for
1082 PCR-based tagging of yeast genes: new fluorescent proteins, more markers and
1083 promoter substitution cassettes. Yeast 21: 947-962.

1084 Jenks, M. H., T. W. O'Rourke and D. Reines, 2008 Properties of an intergenic terminator and
1085 start site switch that regulate IMD2 transcription in yeast. Mol Cell Biol 28: 3883-3893.
1086 Jin, H., and C. D. Kaplan, 2014 Relationships of RNA polymerase II genetic interactors to
1087 transcription start site usage defects and growth in Saccharomyces cerevisiae. G3
1088 (Bethesda) 5: 21-33.
1089 Kadonaga, J. T., 1990 Assembly and disassembly of the Drosophila RNA polymerase II
1090 complex during transcription. J Biol Chem 265: 2624-2631.
1091 Kadonaga, J. T., 2012 Perspectives on the RNA polymerase II core promoter. Wiley Interdiscip
1092 Rev Dev Biol 1: 40-51.
1093 Kaplan, C. D., 2013 Basic mechanisms of RNA polymerase II activity and alteration of gene
1094 expression in Saccharomyces cerevisiae. Biochim Biophys Acta 1829: 39-54.
1095 Kaplan, C. D., M. J. Holland and F. Winston, 2005 Interaction between transcription elongation
1096 factors and mRNA 3'-end formation at the Saccharomyces cerevisiae GAL10-GAL7
1097 locus. J Biol Chem 280: 913-922.
1098 Kaplan, C. D., H. Jin, I. L. Zhang and A. Belyanin, 2012 Dissection of Pol II trigger loop function
1099 and Pol II activity-dependent control of start site selection in vivo. PLoS Genet 8:
1100 e1002627.
1101 Kaplan, C. D., L. Laprade and F. Winston, 2003 Transcription elongation factors repress
1102 transcription initiation from cryptic sites. Science 301: 1096-1099.
1103 Kaster, B. C., K. C. Knippa, C. D. Kaplan and D. O. Peterson, 2016 RNA Polymerase II Trigger
1104 Loop Mobility: INDIRECT EFFECTS OF Rpb9. J Biol Chem 291: 14883-14895.
1105 Khaperskyy, D. A., M. L. Ammerman, R. C. Majovski and A. S. Ponticelli, 2008 Functions of
1106 Saccharomyces cerevisiae TFIIF during transcription start site utilization. Mol Cell Biol
1107 28: 3757-3766.
1108 Kim, J. S., C. Saint-Andre, H. S. Lim, C. S. Hwang, J. M. Egly *et al.*, 2015 Crystal structure of
1109 the Rad3/XPD regulatory domain of Ssl1/p44. J Biol Chem 290: 8321-8330.
1110 Klopotowski, T., and A. Wiater, 1965 Synergism of aminotriazole and phosphate on the
1111 inhibition of yeast imidazole glycerol phosphate dehydratase. Arch Biochem Biophys
1112 112: 562-566.
1113 Knaus, R., R. Pollock and L. Guarente, 1996 Yeast SUB1 is a suppressor of TFIIB mutations
1114 and has homology to the human co-activator PC4. EMBO J 15: 1933-1940.
1115 Kopcewicz, K. A., T. W. O'Rourke and D. Reines, 2007 Metabolic regulation of IMD2
1116 transcription and an unusual DNA element that generates short transcripts. Mol Cell Biol
1117 27: 2821-2829.
1118 Kornberg, R. D., 2007 The molecular basis of eukaryotic transcription. Proc Natl Acad Sci U S A
1119 104: 12955-12961.
1120 Kostrewa, D., M. E. Zeller, K. J. Armache, M. Seizl, K. Leike *et al.*, 2009 RNA polymerase II-
1121 TFIIB structure and mechanism of transcription initiation. Nature 462: 323-330.
1122 Kubicek, C. E., R. D. Chisholm, S. Takayama and D. K. Hawley, 2013 RNA polymerase II
1123 mutations conferring defects in poly(A) site cleavage and termination in Saccharomyces
1124 cerevisiae. G3 (Bethesda) 3: 167-180.
1125 Kuehner, J. N., and D. A. Brow, 2006 Quantitative analysis of in vivo initiator selection by yeast
1126 RNA polymerase II supports a scanning model. J Biol Chem 281: 14119-14128.
1127 Kuehner, J. N., and D. A. Brow, 2008 Regulation of a eukaryotic gene by GTP-dependent start
1128 site selection and transcription attenuation. Mol Cell 31: 201-211.
1129 Langmead, B., and S. L. Salzberg, 2012 Fast gapped-read alignment with Bowtie 2. Nat
1130 Methods 9: 357-359.
1131 Laughery, M. F., T. Hunter, A. Brown, J. Hoopes, T. Ostbye *et al.*, 2015 New vectors for simple
1132 and streamlined CRISPR-Cas9 genome editing in Saccharomyces cerevisiae. Yeast 32:
1133 711-720.

1134 Li, H., B. Handsaker, A. Wysoker, T. Fennell, J. Ruan *et al.*, 2009 The Sequence
1135 Alignment/Map format and SAMtools. Bioinformatics 25**:** 2078-2079.
1136 Lifton, R. P., M. L. Goldberg, R. W. Karp and D. S. Hogness, 1978 The organization of the
1137 histone genes in Drosophila melanogaster: functional and evolutionary implications. Cold
1138 Spring Harb Symp Quant Biol 42 Pt 2**:** 1047-1051.
1139 Lin, Y. C., and J. D. Gralla, 2005 Stimulation of the XPB ATP-dependent helicase by the beta
1140 subunit of TFIIE. Nucleic Acids Res 33**:** 3072-3081.
1141 Lu, Z., and Z. Lin, 2019 Pervasive and dynamic transcription initiation in Saccharomyces
1142 cerevisiae. Genome Res 29**:** 1198-1210.
1143 Lu, Z., and Z. Lin, 2021 The origin and evolution of a distinct mechanism of transcription
1144 initiation in yeasts. Genome Res 31**:** 51-63.
1145 Luse, D. S., M. Parida, B. M. Spector, K. A. Nilson and D. H. Price, 2020 A unified view of the
1146 sequence and functional organization of the human RNA polymerase II promoter.
1147 Nucleic Acids Res 48**:** 7767-7785.
1148 Malabat, C., F. Feuerbach, L. Ma, C. Saveanu and A. Jacquier, 2015 Quality control of
1149 transcription start site selection by nonsense-mediated-mRNA decay. Elife 4.
1150 Malik, I., C. Qiu, T. Snavely and C. D. Kaplan, 2017 Wide-ranging and unexpected
1151 consequences of altered Pol II catalytic activity in vivo. Nucleic Acids Res 45**:** 4431-
1152 4451.
1153 Malone, E. A., C. D. Clark, A. Chiang and F. Winston, 1991 Mutations in SPT16/CDC68
1154 suppress cis- and trans-acting mutations that affect promoter function in Saccharomyces
1155 cerevisiae. Mol Cell Biol 11**:** 5710-5717.
1156 Mandal, D., T. B. Woolf and R. Rao, 2000 Manganese selectivity of pmr1, the yeast secretory
1157 pathway ion pump, is defined by residue gln783 in transmembrane segment 6. Residue
1158 Asp778 is essential for cation transport. J Biol Chem 275**:** 23933-23938.
1159 Mani, R., R. P. St Onge, J. L. t. Hartman, G. Giaever and F. P. Roth, 2008 Defining genetic
1160 interaction. Proc Natl Acad Sci U S A 105**:** 3461-3466.
1161 Martens, J. A., L. Laprade and F. Winston, 2004 Intergenic transcription is required to repress
1162 the Saccharomyces cerevisiae SER3 gene. Nature 429**:** 571-574.
1163 Martin, M., 2011 Cutadapt removes adapter sequences from high-throughput sequencing reads.
1164 2011 17**:** 3.
1165 Miller, G., and S. Hahn, 2006 A DNA-tethered cleavage probe reveals the path for promoter
1166 DNA in the yeast preinitiation complex. Nat Struct Mol Biol 13**:** 603-610.
1167 Miura, F., N. Kawaguchi, J. Sese, A. Toyoda, M. Hattori *et al.*, 2006 A large-scale full-length
1168 cDNA analysis to explore the budding yeast transcriptome. Proc Natl Acad Sci U S A
1169 103**:** 17846-17851.
1170 Murakami, K., P. J. Mattei, R. E. Davis, H. Jin, C. D. Kaplan *et al.*, 2015 Uncoupling Promoter
1171 Opening from Start-Site Scanning. Mol Cell 59**:** 133-138.
1172 Na, J. G., I. Pinto and M. Hampsey, 1992 Isolation and characterization of SUA5, a novel gene
1173 required for normal growth in Saccharomyces cerevisiae. Genetics 131**:** 791-801.
1174 Nagalakshmi, U., Z. Wang, K. Waern, C. Shou, D. Raha *et al.*, 2008 The transcriptional
1175 landscape of the yeast genome defined by RNA sequencing. Science 320**:** 1344-1349.
1176 Namjilsuren, S., and K. M. Arndt, 2025 Glc7/PP1 triggers Paf1 complex dissociation from RNA
1177 polymerase II to enable transcription termination. bioRxiv.
1178 Niyogi, S. K., R. P. Feldman and D. J. Hoffman, 1981 Selective effects of metal ions on RNA
1179 synthesis rates. Toxicology 22**:** 9-21.
1180 Orphanides, G., T. Lagrange and D. Reinberg, 1996 The general transcription factors of RNA
1181 polymerase II. Genes Dev 10**:** 2657-2683.
1182 Pardee, T. S., C. S. Bangur and A. S. Ponticelli, 1998 The N-terminal region of yeast TFIIB
1183 contains two adjacent functional domains involved in stable RNA polymerase II binding
1184 and transcription start site selection. J Biol Chem 273**:** 17859-17864.

1185 Park, D., A. R. Morris, A. Battenhouse and V. R. Iyer, 2014 Simultaneous mapping of transcript
1186 ends at single-nucleotide resolution and identification of widespread promoter-
1187 associated non-coding RNA governed by TATA elements. Nucleic Acids Res 42: 3736-
1188 3749.
1189 Pau, G., F. Fuchs, O. Sklyar, M. Boutros and W. Huber, 2010 EBImage--an R package for
1190 image processing with applications to cellular phenotypes. Bioinformatics 26: 979-981.
1191 Pelechano, V., W. Wei and L. M. Steinmetz, 2013 Extensive transcriptional heterogeneity
1192 revealed by isoform profiling. Nature 497: 127-131.
1193 Pinto, I., J. G. Na, F. Sherman and M. Hampsey, 1992a cis- and trans-acting suppressors of a
1194 translation initiation defect at the cyc1 locus of Saccharomyces cerevisiae. Genetics
1195 132: 97-112.
1196 Pinto, I., D. E. Ware and M. Hampsey, 1992b The yeast SUA7 gene encodes a homolog of
1197 human transcription factor TFIIB and is required for normal start site selection in vivo.
1198 Cell 68: 977-988.
1199 Pinto, I., W. H. Wu, J. G. Na and M. Hampsey, 1994 Characterization of sua7 mutations defines
1200 a domain of TFIIB involved in transcription start site selection in yeast. J Biol Chem 269:
1201 30569-30573.
1202 Policastro, R. A., D. J. McDonald, V. P. Brendel and G. E. Zentner, 2021 Flexible analysis of
1203 TSS mapping data and detection of TSS shifts with TSRexploreR. NAR Genom
1204 Bioinform 3: lqab051.
1205 Policastro, R. A., R. T. Raborn, V. P. Brendel and G. E. Zentner, 2020 Simple and efficient
1206 profiling of transcription initiation and transcript levels with STRIPE-seq. Genome Res
1207 30: 910-923.
1208 Policastro, R. A., and G. E. Zentner, 2022 Genome-Wide Profiling of Transcription Initiation with
1209 STRIPE-seq. Methods Mol Biol 2477: 21-34.
1210 Powers, E. N., C. Chan, E. Doron-Mandel, L. Llacsahuanga Allcca, J. Kim Kim *et al.*, 2022
1211 Bidirectional promoter activity from expression cassettes can drive off-target repression
1212 of neighboring gene translation. Elife 11.
1213 Prelich, G., and F. Winston, 1993 Mutations that suppress the deletion of an upstream activating
1214 sequence in yeast: involvement of a protein kinase and histone H3 in repressing
1215 transcription in vivo. Genetics 135: 665-676.
1216 Qiu, C., P. Arora, I. Malik, A. J. Laperuta, E. M. Pavlovic *et al.*, 2024 Thiolutin has complex
1217 effects in vivo but is a direct inhibitor of RNA polymerase II in vitro. Nucleic Acids Res
1218 52: 2546-2564.
1219 Qiu, C., O. C. Erinne, J. M. Dave, P. Cui, H. Jin *et al.*, 2016 High-Resolution Phenotypic
1220 Landscape of the RNA Polymerase II Trigger Loop. PLoS Genet 12: e1006321.
1221 Qiu, C., H. Jin, I. Vvedenskaya, J. A. Llenas, T. Zhao *et al.*, 2020 Universal promoter scanning
1222 by Pol II during transcription initiation in Saccharomyces cerevisiae. Genome Biol 21:
1223 132.
1224 Rando, O. J., and F. Winston, 2012 Chromatin and transcription in yeast. Genetics 190: 351-
1225 387.
1226 Rhee, H. S., and B. F. Pugh, 2012 Genome-wide structure and organization of eukaryotic pre-
1227 initiation complexes. Nature 483: 295-301.
1228 Roeder, R. G., 1996 The role of general initiation factors in transcription by RNA polymerase II.
1229 Trends Biochem Sci 21: 327-335.
1230 Roeder, R. G., 2019 50+ years of eukaryotic transcription: an expanding universe of factors and
1231 mechanisms. Nat Struct Mol Biol 26: 783-791.
1232 Rudolph, H. K., A. Antebi, G. R. Fink, C. M. Buckley, T. E. Dorman *et al.*, 1989 The yeast
1233 secretory pathway is perturbed by mutations in PMR1, a member of a Ca2+ ATPase
1234 family. Cell 58: 133-145.

1235 Sainsbury, S., J. Niesser and P. Cramer, 2013 Structure and function of the initially transcribing
1236 RNA polymerase II-TFIIB complex. Nature 493**:** 437-440.
1237 Sandelin, A., P. Carninci, B. Lenhard, J. Ponjavic, Y. Hayashizaki *et al.*, 2007 Mammalian RNA
1238 polymerase II core promoters: insights from genome-wide studies. Nat Rev Genet 8**:**
1239 424-436.
1240 Schilbach, S., S. Aibara, C. Dienemann, F. Grabbe and P. Cramer, 2021 Structure of RNA
1241 polymerase II pre-initiation complex at 2.9 A defines initial DNA opening. Cell 184**:** 4064-
1242 4072 e4028.
1243 Schilbach, S., M. Hantsche, D. Tegunov, C. Dienemann, C. Wigge *et al.*, 2017 Structures of
1244 transcription pre-initiation complex with TFIIH and Mediator. Nature 551**:** 204-209.
1245 Schmitt, M. E., T. A. Brown and B. L. Trumpower, 1990 A rapid and simple method for
1246 preparation of RNA from Saccharomyces cerevisiae. Nucleic Acids Res 18**:** 3091-3092.
1247 Sikorski, T. W., S. B. Ficarro, J. Holik, T. Kim, O. J. Rando *et al.*, 2011 Sub1 and RPA associate
1248 with RNA polymerase II at different stages of transcription. Mol Cell 44**:** 397-409.
1249 Simchen, G., F. Winston, C. A. Styles and G. R. Fink, 1984 Ty-mediated gene expression of the
1250 LYS2 and HIS4 genes of Saccharomyces cerevisiae is controlled by the same SPT
1251 genes. Proc Natl Acad Sci U S A 81**:** 2431-2434.
1252 Smale, S. T., and J. T. Kadonaga, 2003 The RNA polymerase II core promoter. Annu Rev
1253 Biochem 72**:** 449-479.
1254 Smith, T., A. Heger and I. Sudbery, 2017 UMI-tools: modeling sequencing errors in Unique
1255 Molecular Identifiers to improve quantification accuracy. Genome Res 27**:** 491-499.
1256 Struhl, K., 1987 Promoters, activator proteins, and the mechanism of transcriptional initiation in
1257 yeast. Cell 49**:** 295-297.
1258 Struhl, K., and R. W. Davis, 1977 Production of a functional eukaryotic enzyme in Escherichia
1259 coli: cloning and expression of the yeast structural gene for imidazole-glycerolphosphate
1260 dehydratase (his3). Proc Natl Acad Sci U S A 74**:** 5255-5259.
1261 Sun, Z. W., and M. Hampsey, 1995 Identification of the gene (SSU71/TFG1) encoding the
1262 largest subunit of transcription factor TFIIF as a suppressor of a TFIIB mutation in
1263 Saccharomyces cerevisiae. Proc Natl Acad Sci U S A 92**:** 3127-3131.
1264 Sun, Z. W., and M. Hampsey, 1996 Synthetic enhancement of a TFIIB defect by a mutation in
1265 SSU72, an essential yeast gene encoding a novel protein that affects transcription start
1266 site selection in vivo. Mol Cell Biol 16**:** 1557-1566.
1267 Sun, Z. W., A. Tessmer and M. Hampsey, 1996 Functional interaction between TFIIB and the
1268 Rpb9 (Ssu73) subunit of RNA polymerase II in Saccharomyces cerevisiae. Nucleic Acids
1269 Res 24**:** 2560-2566.
1270 Swanson, M. S., E. A. Malone and F. Winston, 1991 SPT5, an essential gene important for
1271 normal transcription in Saccharomyces cerevisiae, encodes an acidic nuclear protein
1272 with a carboxy-terminal repeat. Mol Cell Biol 11**:** 3009-3019.
1273 Tomko, E. J., J. Fishburn, S. Hahn and E. A. Galburt, 2017 TFIIH generates a six-base-pair
1274 open complex during RNAP II transcription initiation and start-site scanning. Nat Struct
1275 Mol Biol 24**:** 1139-1145.
1276 Tomko, E. J., O. Luyties, J. K. Rimel, C. L. Tsai, J. O. Fuss *et al.*, 2021 The Role of XPB/Ssl2
1277 dsDNA Translocase Processivity in Transcription Start-site Scanning. J Mol Biol 433**:**
1278 166813.
1279 Vaser, R., S. Adusumalli, S. N. Leng, M. Sikic and P. C. Ng, 2016 SIFT missense predictions for
1280 genomes. Nat Protoc 11**:** 1-9.
1281 Vo Ngoc, L., C. J. Cassidy, C. Y. Huang, S. H. Duttke and J. T. Kadonaga, 2017a The human
1282 initiator is a distinct and abundant element that is precisely positioned in focused core
1283 promoters. Genes Dev 31**:** 6-11.
1284 Vo Ngoc, L., Y. L. Wang, G. A. Kassavetis and J. T. Kadonaga, 2017b The punctilious RNA
1285 polymerase II core promoter. Genes Dev 31**:** 1289-1301.

Wang, M., P. Arora, C. D. Kaplan and D. A. Brow, 2025 Substitutions in RNA-binding protein Hrp1 map a potential interaction surface with the yeast RNA polymerase II elongation complex. bioRxiv.

Winston, F., D. T. Chaleff, B. Valent and G. R. Fink, 1984 Mutations affecting Ty-mediated expression of the HIS4 gene of Saccharomyces cerevisiae. Genetics 107**:** 179-197.

Woychik, N. A., W. S. Lane and R. A. Young, 1991 Yeast RNA polymerase II subunit RPB9 is essential for growth at temperature extremes. J Biol Chem 266**:** 19053-19055.

Wu, W. H., I. Pinto, B. S. Chen and M. Hampsey, 1999 Mutational analysis of yeast TFIIB. A functional relationship between Ssu72 and Sub1/Tsp1 defined by allele-specific interactions with TFIIB. Genetics 153**:** 643-652.

Xie, Y., H. Li, X. Luo, H. Li, Q. Gao *et al.*, 2022 IBS 2.0: an upgraded illustrator for the visualization of biological sequences. Nucleic Acids Res 50**:** W420-W426.

Xu, Z., W. Wei, J. Gagneur, F. Perocchi, S. Clauder-Munster *et al.*, 2009 Bidirectional promoters generate pervasive transcription in yeast. Nature 457**:** 1033-1037.

Yang, C., P. Basnet, S. Sharmin, H. Shen, C. D. Kaplan *et al.*, 2024 Transcription start site scanning requires the fungi-specific hydrophobic loop of Tfb3. Nucleic Acids Res 52**:** 11602-11611.

Yang, C., R. Fujiwara, H. J. Kim, P. Basnet, Y. Zhu *et al.*, 2022 Structural visualization of de novo transcription initiation by Saccharomyces cerevisiae RNA polymerase II. Mol Cell 82**:** 660-676 e669.

Yoon, H., S. P. Miller, E. K. Pabich and T. F. Donahue, 1992 SSL1, a suppressor of a HIS4 5'-UTR stem-loop mutation, is essential for translation initiation and affects UV resistance in yeast. Genes Dev 6**:** 2463-2477.

Zhang, Z., and F. S. Dietrich, 2005 Mapping of transcription start sites in Saccharomyces cerevisiae using 5' SAGE. Nucleic Acids Res 33**:** 2838-2851.

Zhao, T., I. O. Vvedenskaya, W. K. Lai, S. Basu, B. F. Pugh *et al.*, 2021 Ssl2/TFIIH function in transcription start site scanning by RNA polymerase II in Saccharomyces cerevisiae. Elife 10.

Zhu, Y., I. O. Vvedenskaya, S. H. Sze, B. E. Nickels and C. D. Kaplan, 2024 Quantitative analysis of transcription start site selection reveals control by DNA sequence, RNA polymerase II activity and NTP levels. Nat Struct Mol Biol 31**:** 190-202.

1319

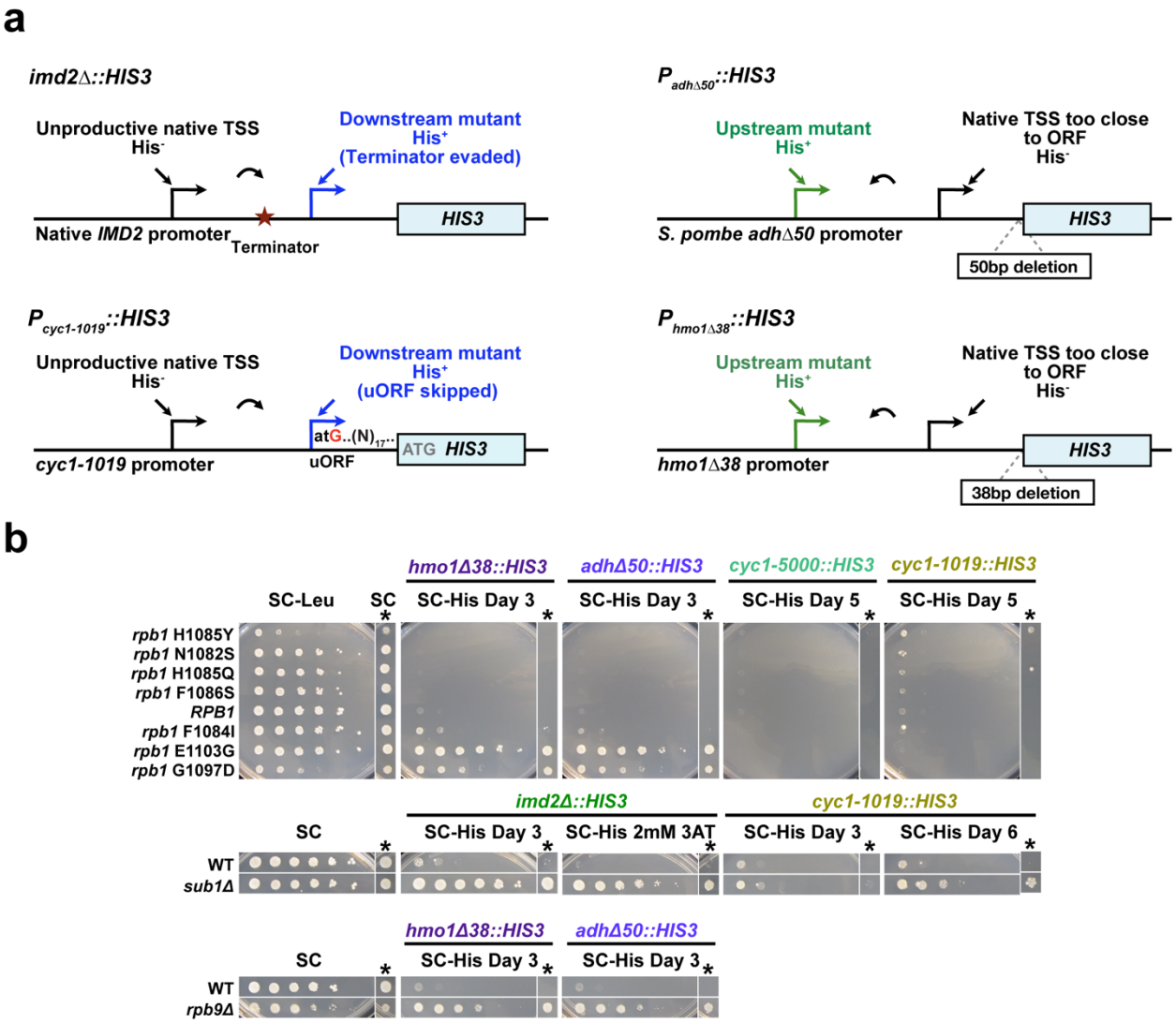


1320

1321 **Figure 1. TSS shift-sensitive reporters detect TSS shifts by *HIS3* expression. a. Left.**
1322 Schematic of initiation reporters *imd2Δ::HIS3* and *cyc1-1019::HIS3* sensitive to downstream
1323 shifts in TSS usage. Downstream-shifting TSS mutants constitutively express *IMD2* transcripts
1324 from a downstream TSS that allows functional *HIS3* expression when *HIS3* replaces the *IMD2*
1325 ORF, conferring a His$^+$ phenotype (top). Downstream TSS shifts at *cyc1-1019::HIS3* allow an
1326 upstream AUG to be bypassed, resulting in usage of the appropriate in-frame AUG, allowing
1327 functional His3p translation (bottom). **Right.** Schematic of the initiation reporters *adhΔ50::HIS3*
1328 (top) and *hmo1Δ38::HIS3* (bottom) that are sensitive to upstream shifts in TSS usage.
1329 Truncation places the native TSSs for these promoters too close to the native AUG rendering
1330 ineffective translation initiation. Upstream shifts in TSS selection lengthen the 5′ UTRs for each
1331 reporter, allowing His3p to be translated from the lengthened *HIS3* mRNA. **b.** Validation of
1332 reporter phenotypes with known TSS-shifting mutants: 10-fold serially diluted yeast strains or a
1333 single concentration of cells (marked with asterisk – "single spot phenotyping") are plated on
1334 media to illustrate reporter function. Here, the *cyc1-5000* allele-based reporter was deployed for
1335 isolating *sua* alleles, where the *cyc1-5000* allele resembles *cyc1-1019* allele (1a, left),
1336 possessing additional C→A and C→G mutations at -23 and -17 positions respectively, relative

to +1 A of the native ATG. This makes the context flanking the upstream AUG start codon more preferred, making the *cyc1-5000* downstream shift detection more stringent than the *cyc1-1019* reporter. *rpb1* alleles (upstream or downstream shifts), *sub1*Δ (downstream shift), and *rpb9*Δ (upstream shift) mutants were tested against the upstream and downstream shift sensitive reporters to illustrate allele-specific reporter activity. Note that *cyc1-1019::HIS3* can be expressed by strong downstream shifting *sub1*Δ and *rpb1* H1085Y of all downstream *rpb1* mutations tested.

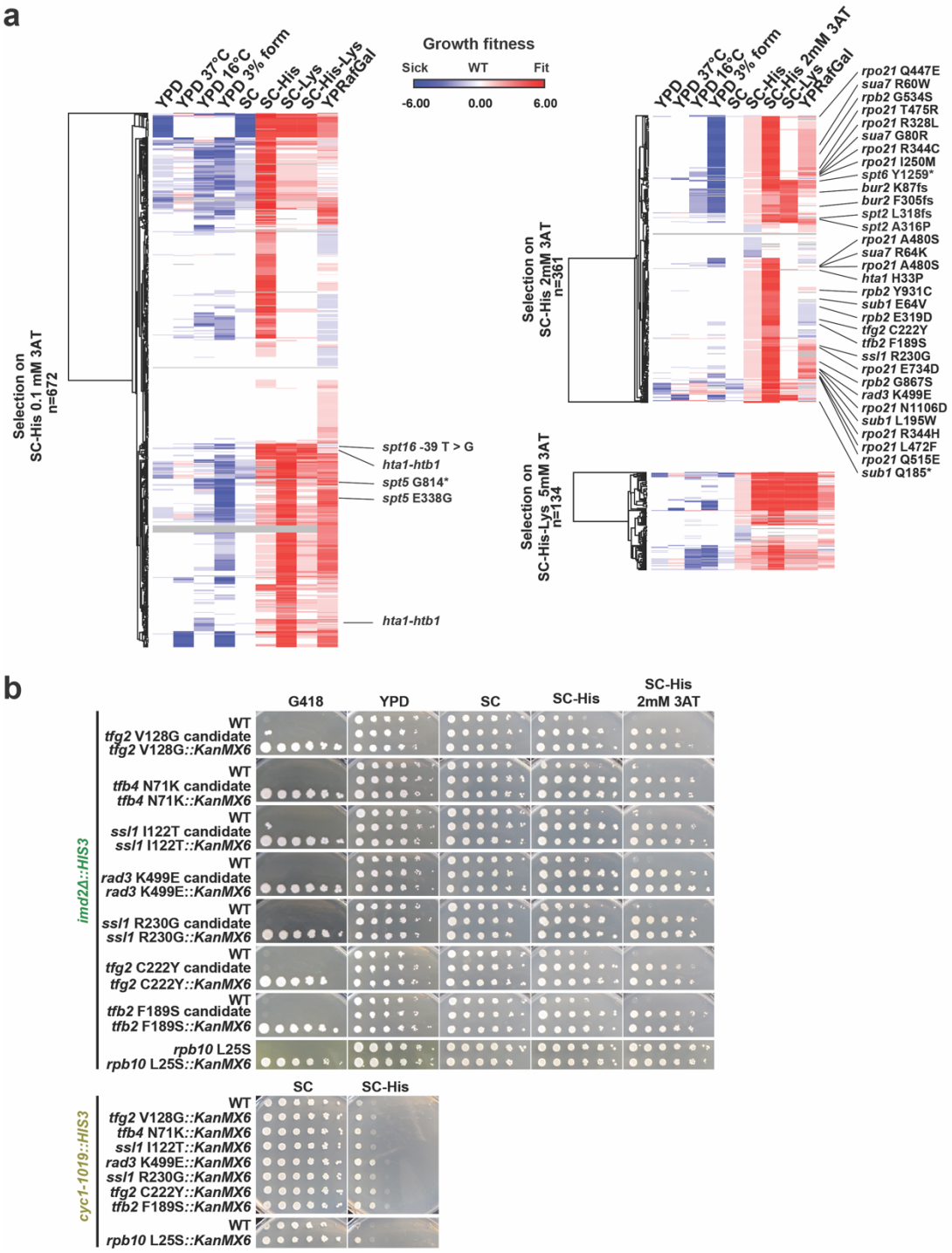

1345 **Figure 2. Isolation of spontaneous suppressors of downstream TSS-shift sensitive**
1346 **initiation reporters. a**. Hierarchically clustered growth phenotypes for a subset of candidate
1347 downstream-shifting suppressors of *cyc1-1019::HIS3* (left) or *imd2Δ::HIS3* (right) reporters with
1348 a subset of identified mutations annotated; right bottom panel displays *imd2Δ::HIS3*
1349 suppressors isolated by selection on SC-His-Lys+5mM 3AT. Phenotypes of candidate
1350 suppressors displayed are relative phenotypes of candidates that have been normalized to
1351 control conditions, as assessed from single-spot phenotyping assays. Phenotypes were scored
1352 from spot assay, corrected to WT and then corrected to the same on control condition (see
1353 Methods). Phenotypic quantification therefore assigns a value of zero for WT-like growth, a
1354 negative value if phenotype is worse than WT and positive, if growth is better than WT and
1355 value of phenotype represents strength of defect. **b.** Validation of a subset of candidates by
1356 knock-in of TSS mutants into *imd2Δ::HIS3* and *cyc1-1019::HIS3* reporter backgrounds and re-
1357 phenotyping. Spot assay phenotyping of candidates isolated from genetic selection (candidate)
1358 and reincorporated mutants with a *kanMX6* tag (*corresponding mutation::kanMX6*) displaying
1359 replication of candidate phenotypes in reincorporated mutants. Mutations were amplified out of
1360 isolated candidates, PCR sewed with a *kanMX6* drug marker cassette and re-introduced into
1361 each of the reporter strains by integrative transformation. The *rpb10* candidate mutation was
1362 introduced using CRISPR/Cas9.

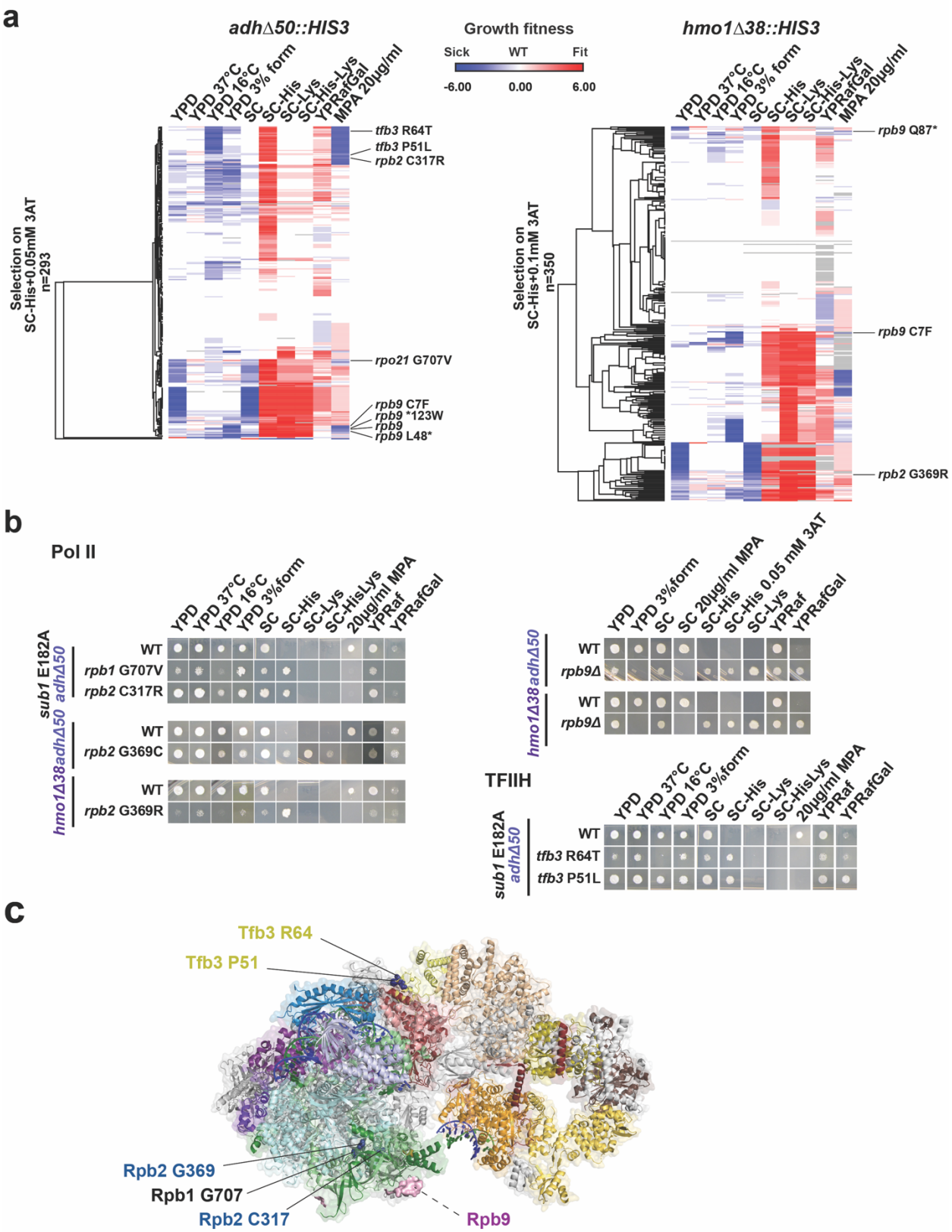


**Figure 3. Isolation of spontaneous suppressors of upstream TSS-shift sensitive initiation reporters. a.** Hierarchically clustered single-spot phenotypes of a subset of upstream-shifting

1366 suppressors of *adhΔ50::HIS3* (left) and *hmo1Δ38::HIS3* (right) initiation reporters with identified
1367 mutations annotated. Phenotypes displayed have been scored and processed as in Fig. 2a.
1368 Briefly, scored phenotypes have been corrected to WT on the same condition, followed by
1369 normalization to the same on control conditions. Here, a positive value represents growth better
1370 than WT and a negative value represents worse than WT (zero). **b.** Single spot phenotyping of
1371 upstream isolated mutants. **c.** Cryo-EM structure of Pol II PIC annotated with upstream shifting
1372 mutation residues identified (PDB: 7O4J).

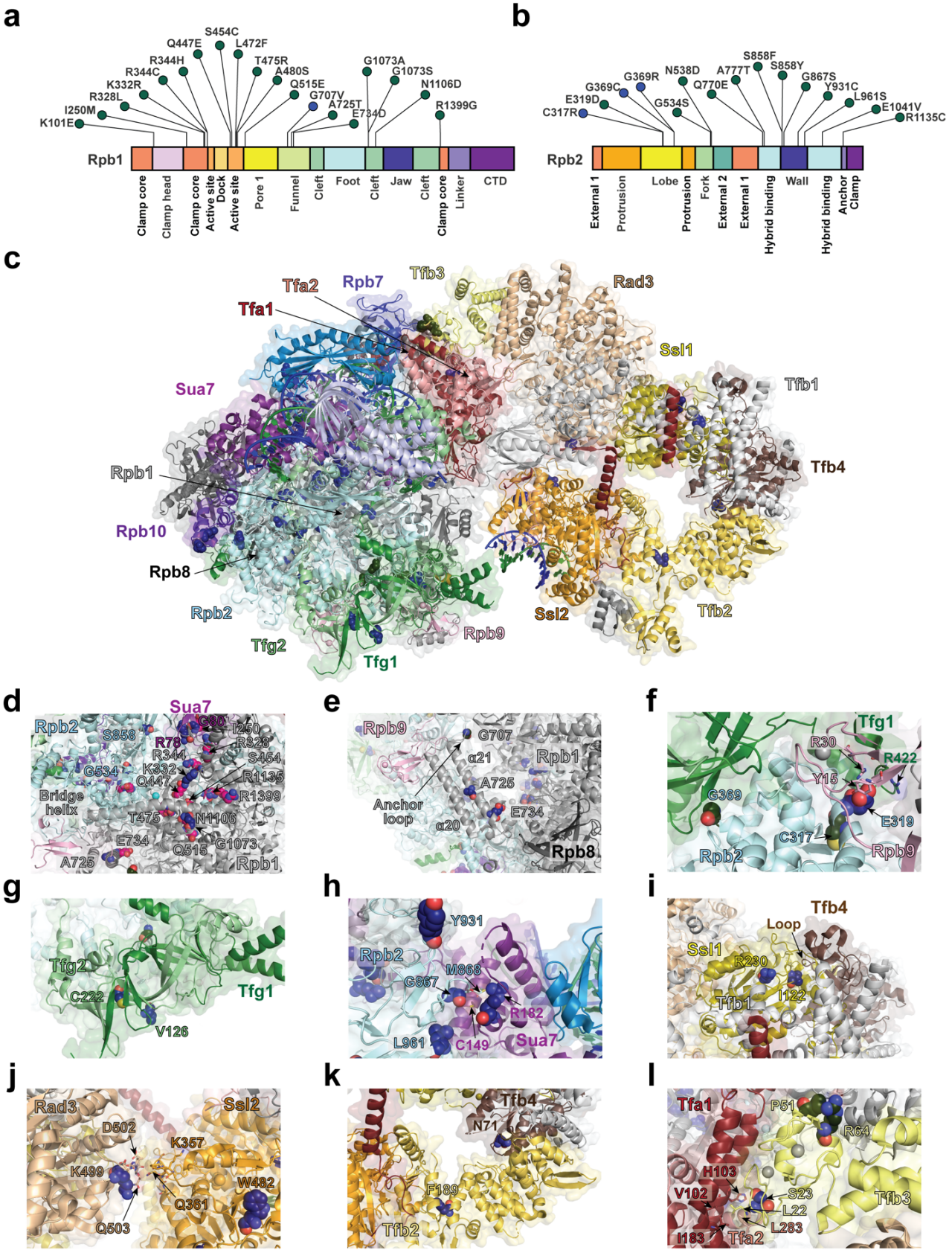
a
S454C
Q447E
L472F
R344H
T475R
R344C
A480S
G1073A
K332R
Q515E
G1073S
R328L
G707V
N1106D
I250M
A725T
R1399G
K101E
E734D
Rpb1
Clamp core
Clamp head
Clamp core
Active site
Dock
Active site
Pore 1
Funnel
Cleft
Foot
Cleft
Jaw
Cleft
Clamp core
Linker
CTD
b
S858F
A777T
S858Y
G867S
G369R
N538D
G369C
Q770E
Y931C
E319D
G534S
L961S
C317R
E1041V
R1135C
Rpb2
External 1
Protrusion
Lobe
Protrusion
Fork
External 2
External 1
Hybrid binding
Wall
Hybrid binding
Anchor
Clamp
c
Tfa2
Rpb7
Tfb3
Rad3
Tfa1
Ssl1
Sua7
Tfb1
Tfb4
Rpb1
Rpb10
Rpb8
Rpb2
Ssl2
Tfb2
Rpb9
Tfg2
Tfg1
d
Sua7
Rpb2
C80
I250
S858
R78
R826
R344
S454
G534
K332
R1135
Q447
R1399
Bridge helix
T475
N1106
E734
G1073
Q515
A725
Rpb1
e
Rpb9
G707
α21
Rpb1
A725
Anchor loop
E734
α20
Rpb8
f
Tfg1
R30
R422
Y15
G369
E319
C317
Rpb2
Rpb9
g
Tfg2
C222
Tfg1
V126
h
Y931
Rpb2
M868
G867
R182
L961
C149
Sua7
i
Tfb4
Loop
Ssl1
R230
I122
Tfb1
j
Rad3
Ssl2
D502
K357
K499
W482
Q361
Q503
k
Tfb4
N71
F189
Tfb2
l
Tfa1
P51
R64
H103
V102
S23
L22
Tfb3
L283
I183
Tfa2

1373

1374 **Figure 4. Mutations identified across PIC**. Lollipop diagram of mutations isolated in Rpb1 (**a**)
1375 and Rpb2 (**b**). Domain diagram figure created using IBS 2.0 (XIE *et al.* 2022). **c**. PIC structure
1376 (PDB: 7O4J) displaying mutations isolated in our study. **d.** Structural mutations surrounding
1377 active cleft that are formamide sensitive marked in magenta. **e.** Mutations in α21 helix and
1378 anchor loop isolated with proximity to Rpb9 and Rpb8. **f.** Residues at Rpb2-TFIIF-Rpb9
1379 interface found to alter TSS selection. **g.** Initiation mutations near Tfg1-Tfg2 interface causing
1380 downstream shifts. **h.** Mutations altering interactions between Sua7 B-core and Rpb2 isolated in
1381 this study in the vicinity of previously isolated Sua7 C149 initiation mutant. **i.** Potential
1382 interactions between Ssl1 and Tfb4 loop or Tfb1 in driving TSS selection. **j.** Rad3 K499E
1383 mutation potentially driving TSS selection by altering interactions with Ssl2 across Rad3-Ssl2
1384 interface with K357R and K357E previously isolated in our study altering TSS selection. **k.**
1385 Mutations in Tfb2 F189 and Tfb4 N71 lying within the respective structural domains potentially
1386 promoting structural "breathing". **l.** Mutation S23F in the RING domain of Tfb3 increasing
1387 interaction between TFIIH and TFIIE by potentially promoting allele-specific hydrophobic
1388 packing.

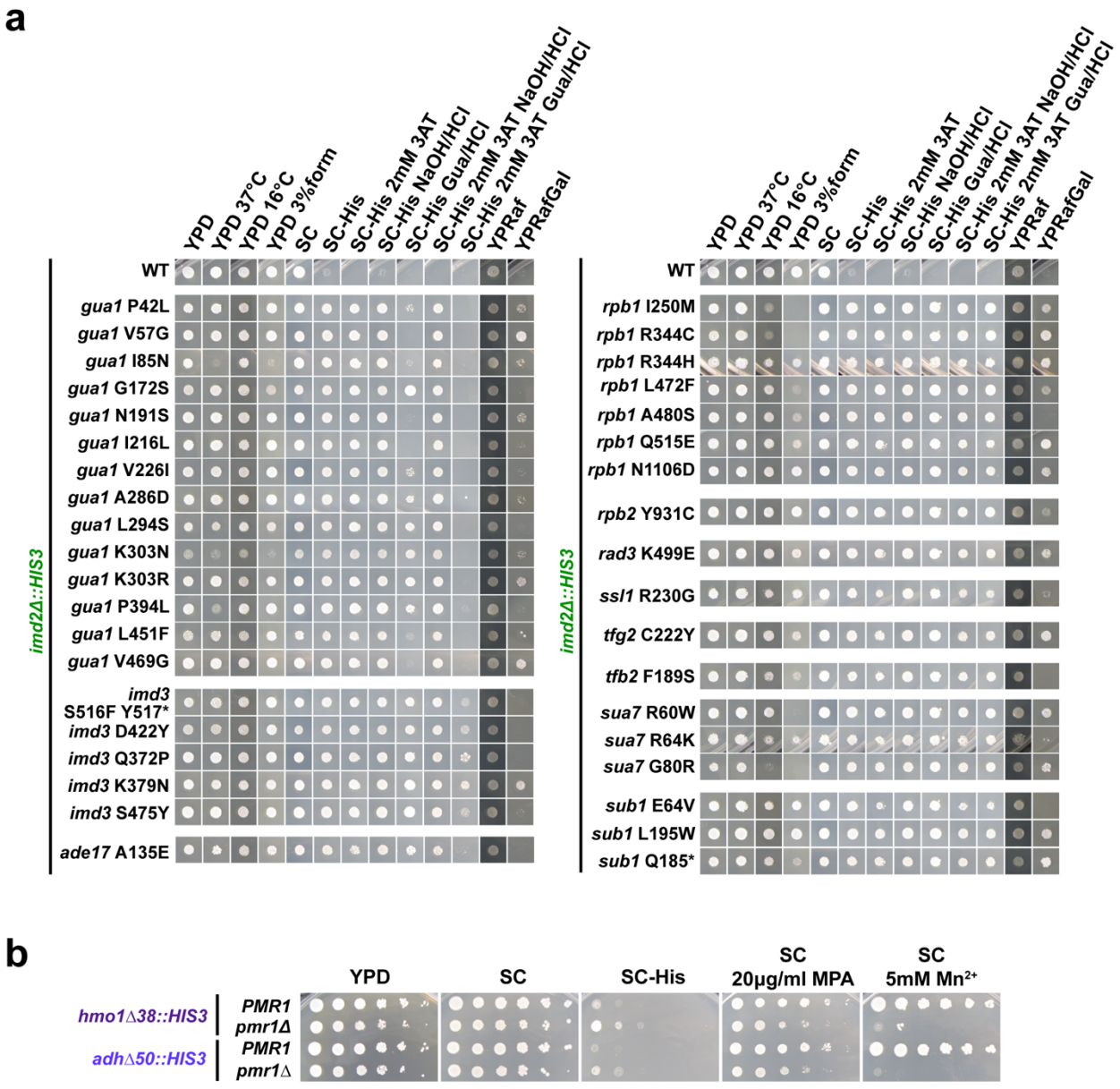


**Figure 5. Phenotyping of subset of non-PIC mutants identified as suppressors of initiation reporters. a.** Guanine metabolism mutants and controls plated as single concentrations of cells on phenotyping media. Guanine metabolism gene mutants confer the His$^+$ phenotype to cells with the *imd2Δ::HIS3* reporter, likely due to the *IMD2* promoter's sensitivity to guanine levels. Guanine supplementation suppresses the His$^+$ phenotype of guanine pathway mutants (SC-His 2 mM 3AT Gua/HCl: left panel) whereas PIC mutants remain His$^+$ under the same conditions (SC-His 2 mM 3AT Gua/HCl: right panel). Guanine is solubilized in 10 mM NaOH at a final concentration of 500 µM and media must be neutralized by equivalent HCl as NaOH alone affects solubility of MPA. **b.** 10-fold serial dilutions of *PMR1* or *pmr1Δ* strains plated on phenotyping media. *pmr1Δ* suppresses both upstream reporters and confers sensitivity to $Mn^{2+}$.

1401

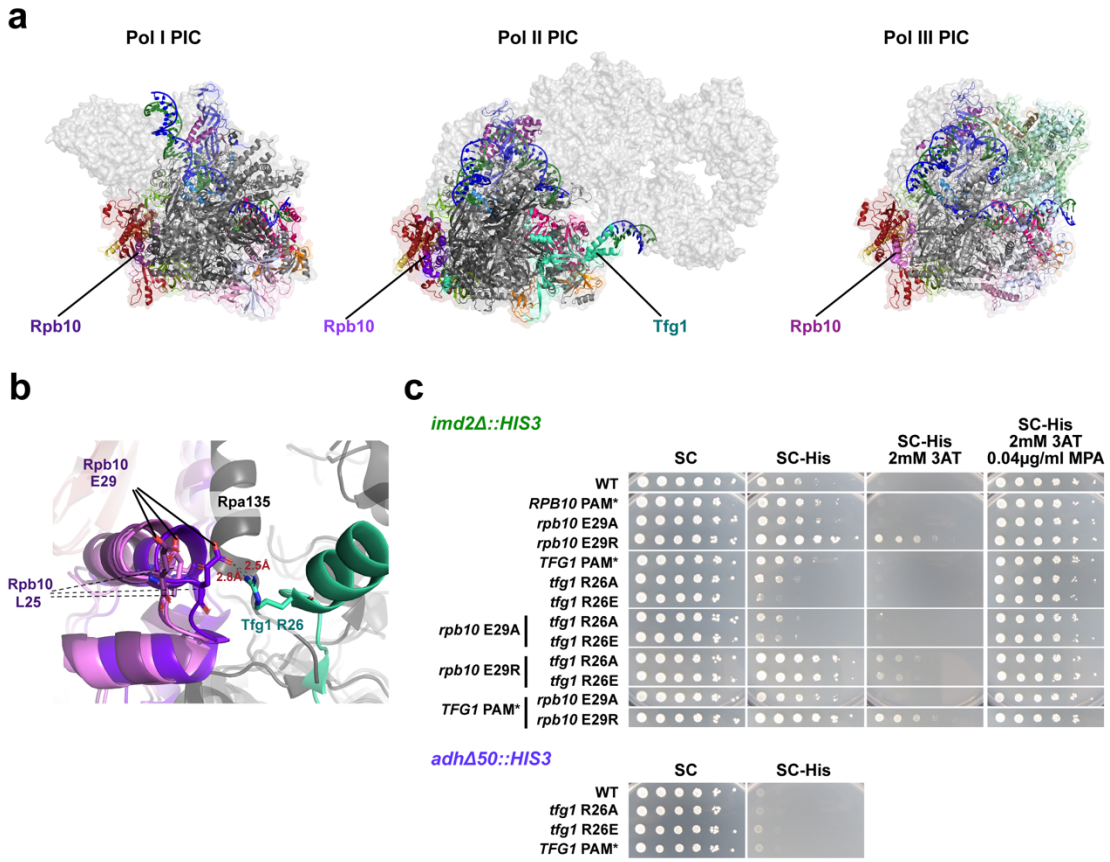


1402

1403 **Figure 6. Analysis of potential Rpb10-Tfg1 interactions in proper TSS selection. a.** Cryo-
1404 EM structures of PICs of Pol I, Pol II, and Pol II displaying Rpb10, a shared subunit between
1405 them. **b.** Cryo-EM structure of Rpb10 from Pol I-III PICs (Pol I PIC: 6TPS, Pol II PIC: 7O4J, Pol
1406 III PIC: 6EU0) overlayed displaying Tfg1 from the Pol II PIC, with Tfg1 R26 in the proximity of
1407 Rpb10 E29 suggesting a potential electrostatic interaction. While Rpa135 in Pol I lies adjacent
1408 to Rpb10, a specific physical interaction with Rpb10 E29 may not exist. **c.** Serially diluted spot
1409 assay phenotyping of single and double mutants of *tfg1* R26 and *rpb10* E29 resides displaying
1410 charge reversals, mutations to alanine and silent PAM control mutations (Rpb10 L30
1411 AAC→AAT) as mutants were generated by CRISPR/Cas9.

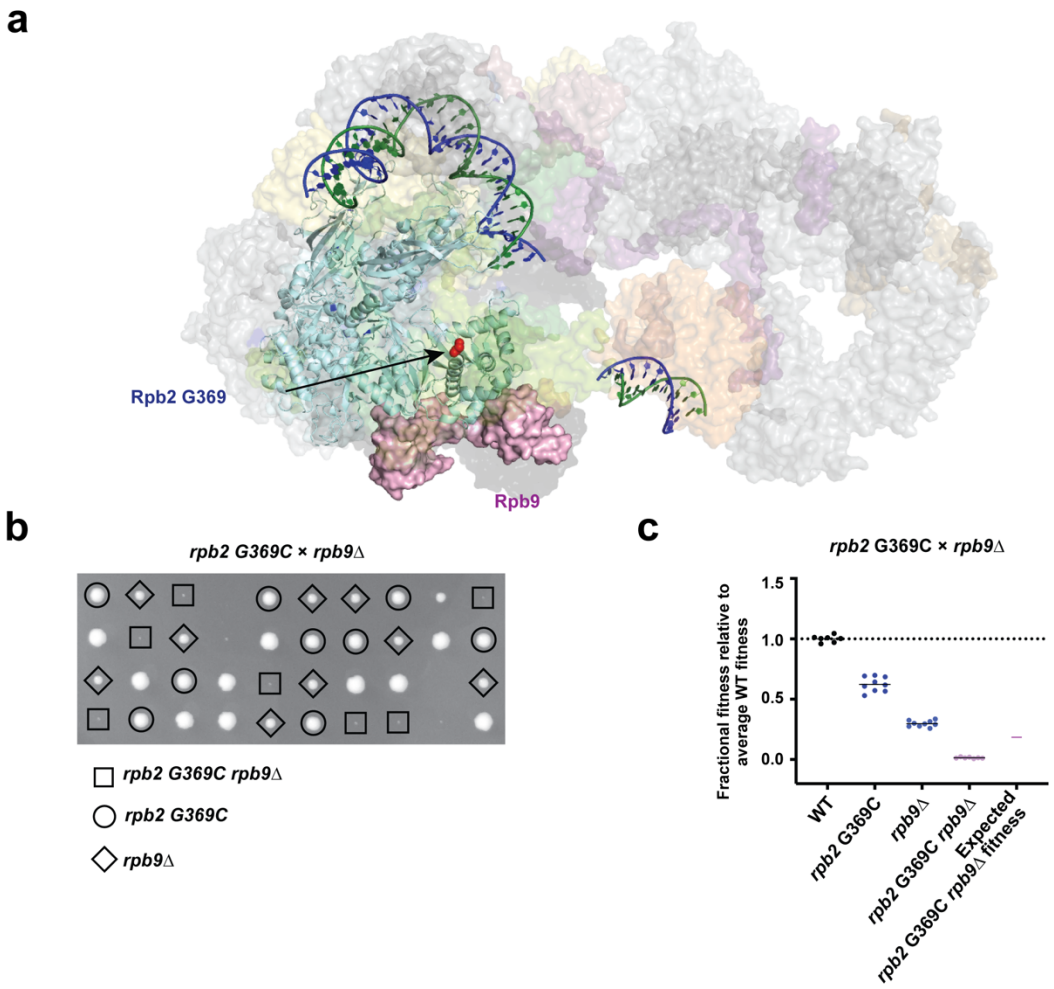


**Figure 7. Synthetic genetic interaction between *rpb9Δ* and *rpb2* G369C. a.** Cryo-EM structure of Pol II PIC displaying Rpb2 G369 and Rpb9. Rpb2 G369 lies in the Pol II lobe domain which interacts with Rpb9 though this region between Rpb2 and Rpb9 and has been shown to interact with TFIIF. **b.** Tetrad dissection of *rpb9Δ*/+ *rpb2* G369C/+ diploid to examine genetic interactions between them. Spores are annotated by genotype. **c.** Observed and expected fitness of single and double mutants plotted for assessing genetic interaction. "Expected" fitness for a double mutant is the product of the two single mutant fitnesses (MANI *et al.* 2008). Observed fitness of single and double mutants estimated by quantification of spore colony sizes. Observed fitness is worse than expected fitness indicating a synthetic genetic interaction.

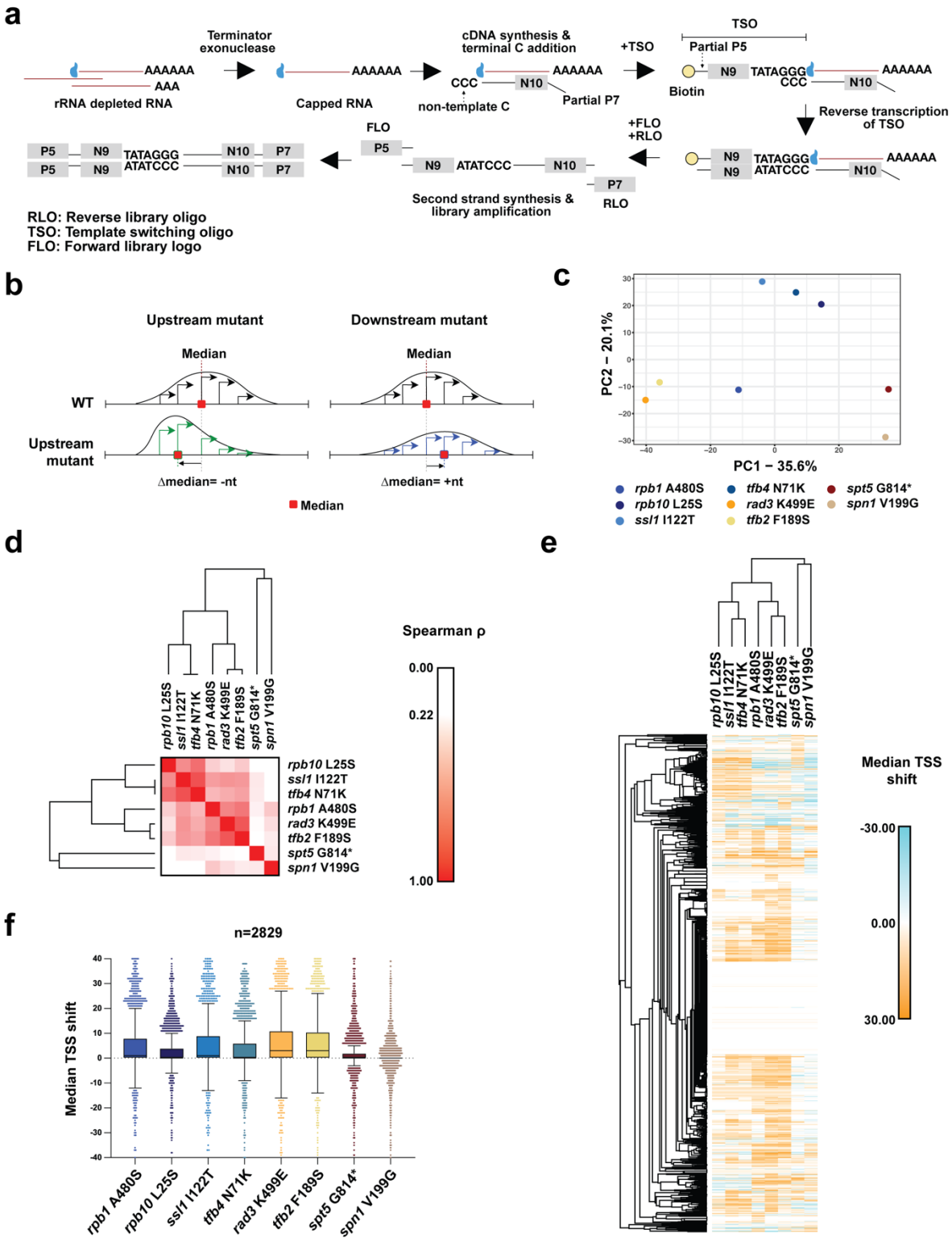
a
Terminator exonuclease
cDNA synthesis & terminal C addition
+TSO
TSO
Partial P5
AAAAAA
AAA
rRNA depleted RNA
Capped RNA
CCC
N10
non-template C
Partial P7
N9
TATAGGG
CCC
Biotin
Reverse transcription of TSO
+FLO
+RLO
FLO
P5
N9
ATATCCC
P7
RLO
Second strand synthesis & library amplification
RLO: Reverse library oligo
TSO: Template switching oligo
FLO: Forward library logo
b
Upstream mutant
Downstream mutant
Median
WT
Upstream mutant
Δmedian= -nt
Δmedian= +nt
Median
c
PC2 – 20.1%
PC1 – 35.6%
rpb1 A480S
rpb10 L25S
ssl1 I122T
tfb4 N71K
rad3 K499E
tfb2 F189S
spt5 G814*
spn1 V199G
d
Spearman ρ
0.00
0.22
1.00
e
Median TSS shift
-30.00
0.00
30.00
f
n=2829
Median TSS shift

1423

1424 **Figure 8. STRIPE-seq analysis of novel mutants identifies three functional groups of**
1425 **initiation mutants based on shift of median of TSS distribution. a.** Schematic of STRIPE-
1426 seq library generation. **b.** Schematic of ∆median metric for TSS analysis. **c.** Principal
1427 component analysis (PCA) of ∆median values of the top 2829 promoters based on an
1428 expression cutoff of ≥10 reads within the analyzed 401 nucleotide promoter windows. PCA of
1429 ∆median values across mutants with combined biological replicates plotted along the first two
1430 principal components display three clusters, ① chromatin mutants *spt5* G814*, *spn1* V199G, ②
1431 *rpb1* A480S, *rpb10* L25S, *ssl1* I122T, *tfb4* N71K and ③ *rad3* K499E and *tfb2* F189S. **d.**
1432 Hierarchical clustering of Spearman correlation of ∆median values across mutants. **e.**
1433 Hierarchically clustered heatmap of ∆median values across top 2829 promoters of mutants with
1434 replicates combined. **f.** Box-plot analysis of ∆median values across mutants presented by Tukey
1435 plot.

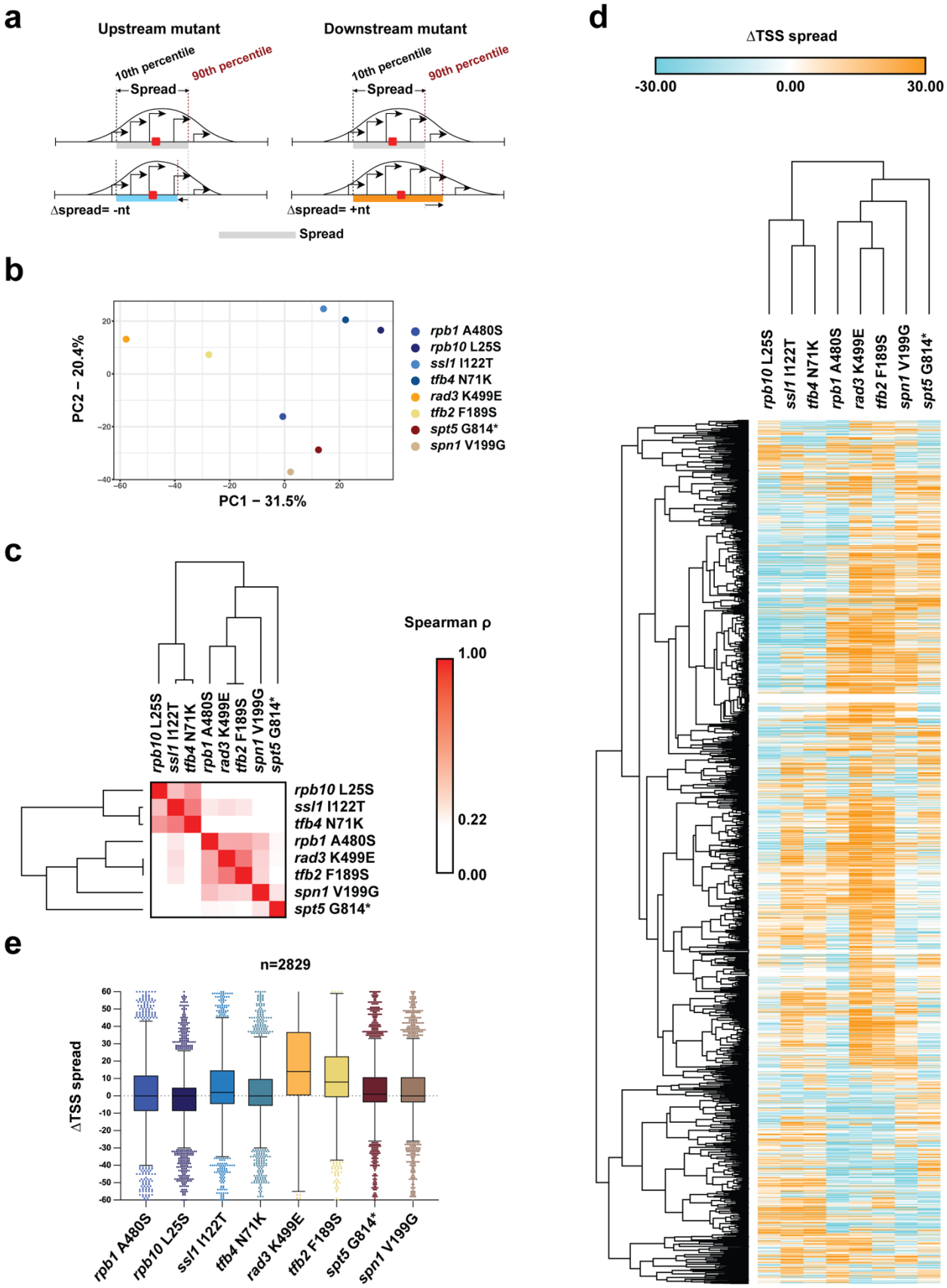
a
Upstream mutant
Downstream mutant
10th percentile
90th percentile
Spread
Δspread= -nt
Δspread= +nt
Spread
b
PC2 – 20.4%
PC1 – 31.5%
rpb1 A480S
rpb10 L25S
ssl1 I122T
tfb4 N71K
rad3 K499E
tfb2 F189S
spt5 G814*
spn1 V199G
c
Spearman ρ
1.00
0.22
0.00
d
ΔTSS spread
-30.00
0.00
30.00
e
n=2829
ΔTSS spread

1436

1437 **Figure 9. STRIPE-seq analysis of novel mutants identifies three functional groups of**
1438 **initiation mutants based on shift of spread of TSS distribution. a.** Schematic of Δspread
1439 metric of analysis **b.** Principal component analysis of Δspread values of top 2829 genes across
1440 mutants plotted along the first two principal components displays three clusters for Δmedian, ①
1441 chromatin mutants *spt5* G814*, *spn1* V199G, ② *rpb1* A480S, *rpb10* L25S, *ssl1* I122T, *tfb4*
1442 N71K and ③ *rad3* K499E and *tfb2* F189S. **c.** Hierarchical clustering of Spearman correlation of
1443 Δspread values across mutants. **d.** Hierarchically clustered heatmap of Δspread values across
1444 top 2829 promoters of mutants. **e.** Box-plot analysis of Δspread values across mutants
1445 presented by Tukey plot.

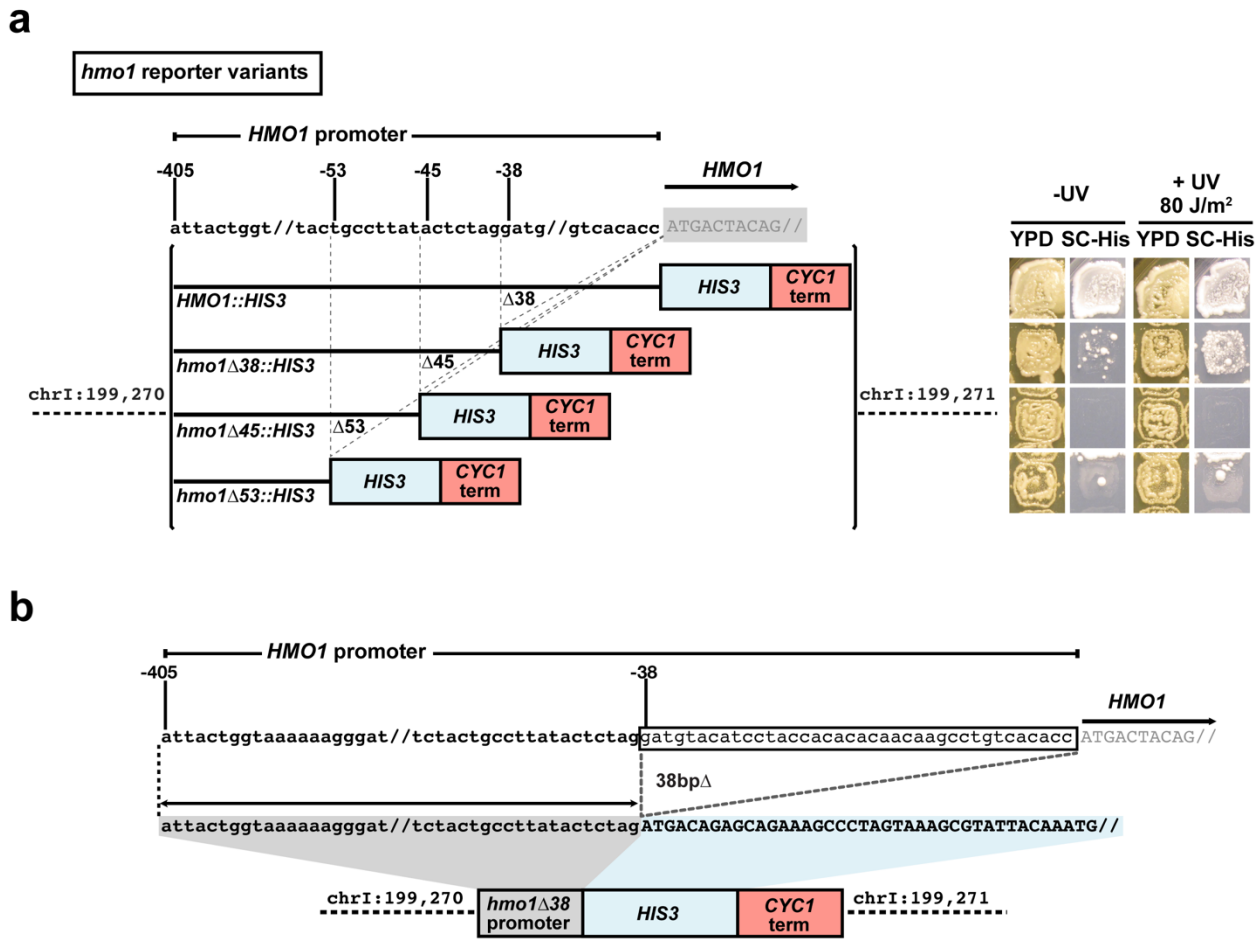


**Figure S1. Isolation of *HMO1* promoter variant that detects upstream TSS shifts. a.** Schematic illustrating an *HMO1* promoter variant deletion series (left) with behavior of reporters in cells in absence or presence of UV mutagenesis (right) to assess potential for His$^+$ mutant generation on the His$^-$ background, indicative of reporter suppression. **b.** Schematic of functional *hmo1Δ38::HIS3* reporter. *HMO1* promoter sequence between –405 and –39 was amplified and appended to the *HIS3* ORF followed by the *CYC1* terminator and integrated into a gene free region of chromosome I (chrI:199270-199271).

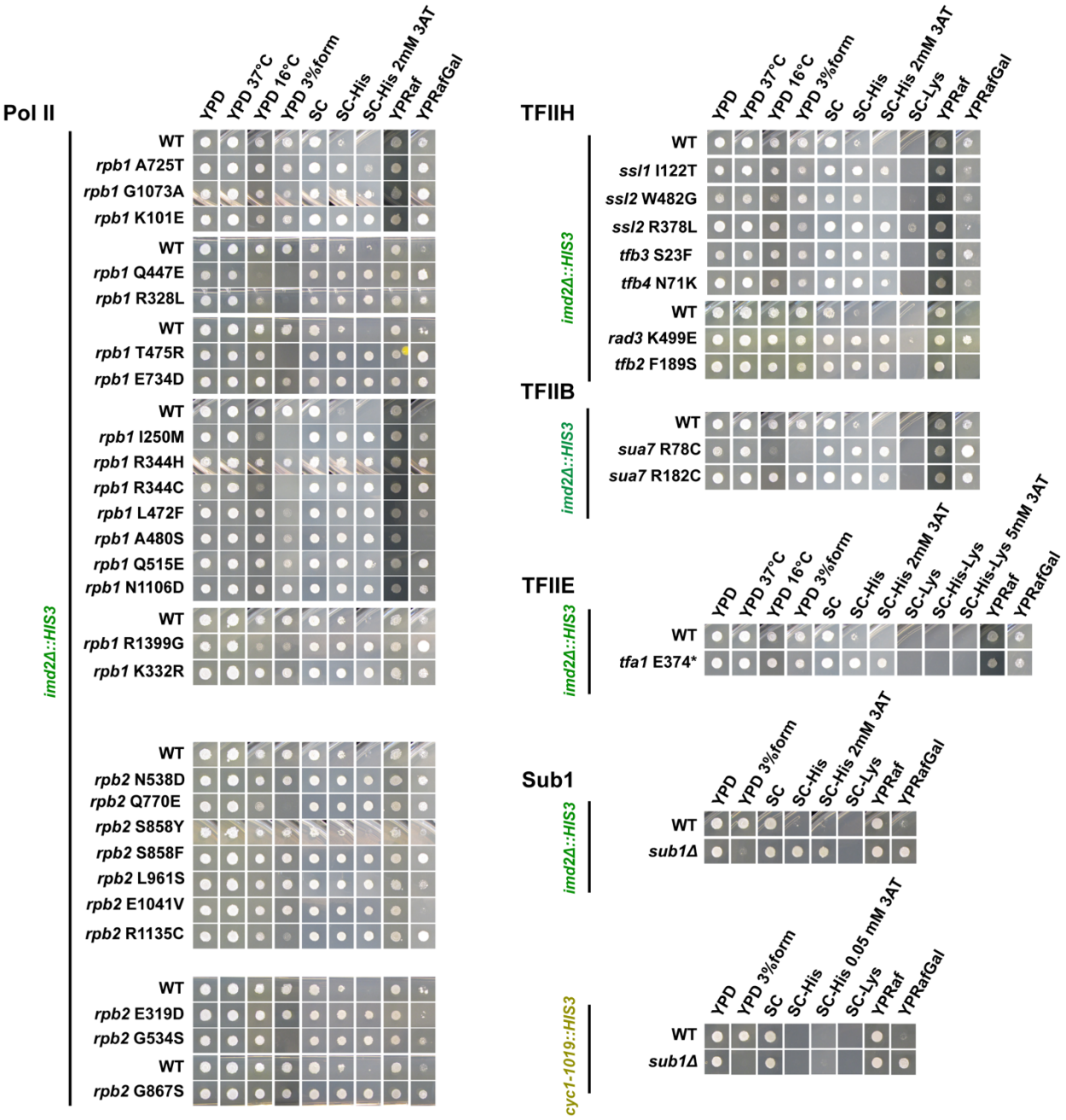


**Figure S2. Initiation and secondary phenotypes of mutants isolated in genetic selections.** Single spot phenotyping of a subset of downstream-shifting mutants isolated in our study.

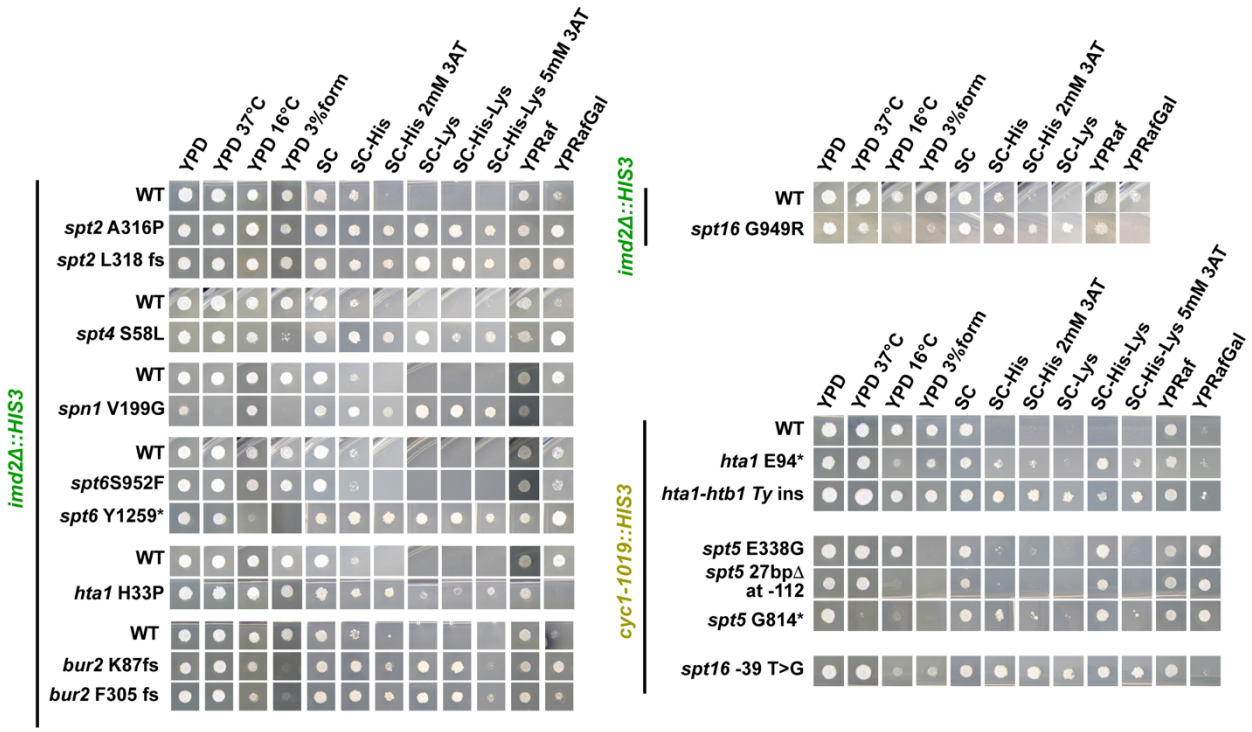


**Figure S3. Phenotypes of chromatin mutants isolated in the study.** Chromatin/Pol II elongation factor mutants identified for both downstream-shift sensitive reporters (subset shown).

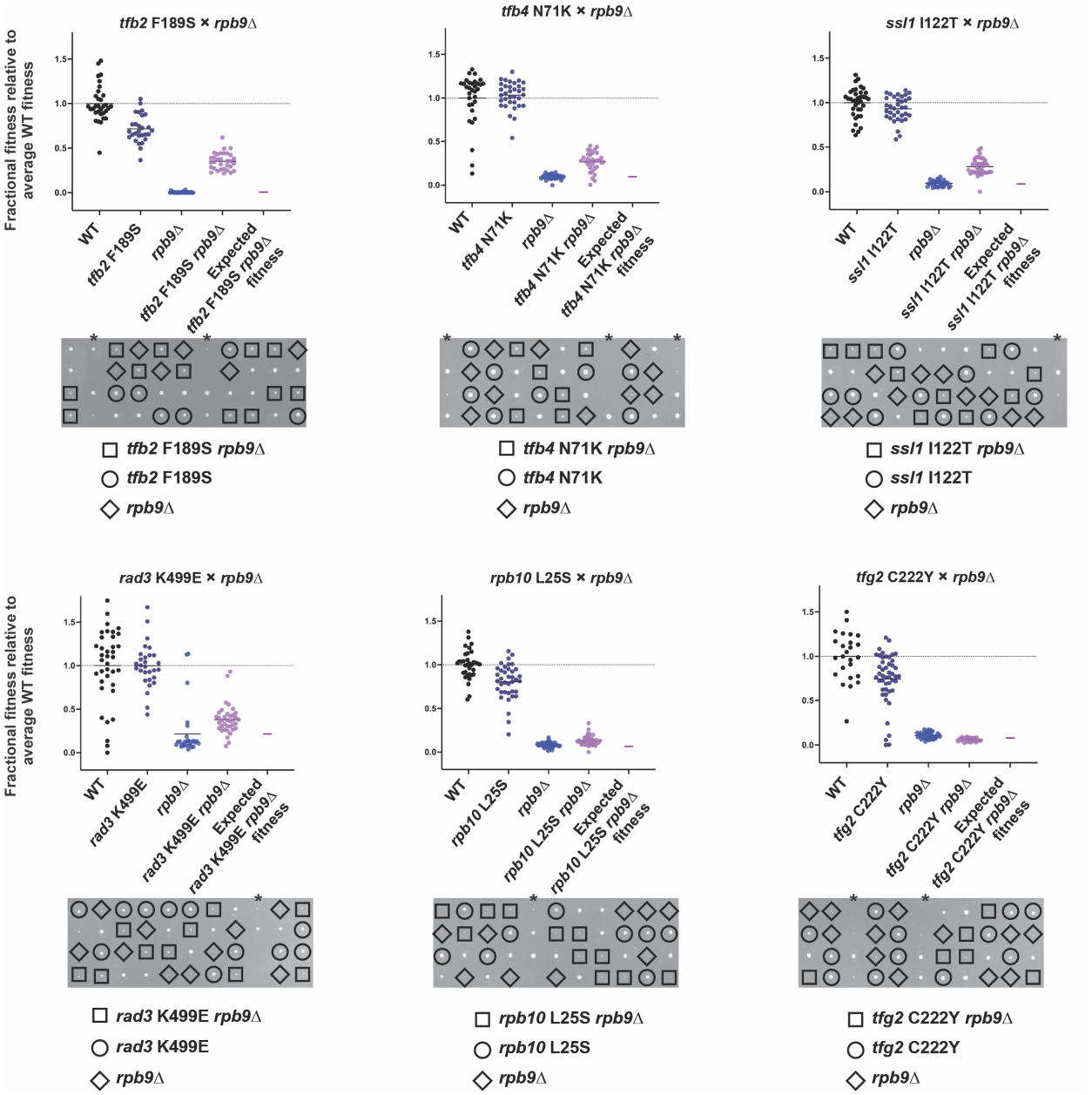


**Figure S4. Genetic interactions between upstream-shifting *rpb9*Δ and novel downstream-shifting alleles prioritized in this study.** Genetic interaction by tetrad analysis between *rpb9*Δ and downstream shifting novel alleles *tfb2* F189S, *tfb4* N71K, *ssl1* I122T across the top (left-right) and *rad3* K499E, *rpb10* L25S and *tfg2* C222Y across the bottom (left-right). Growth phenotypes quantified through spore colony size as in Figure 6. Suppression of *rpb9*Δ fitness defect by *tfb2* F189S, *tfb4* N71K, *ssl1* I122T and *rad3* K499E observed, while interactions with *rpb10* L25S and *tfg2* C222Y appear epistatic. Asterisks (*) indicate incomplete tetrads or failed dissections not considered.

1470

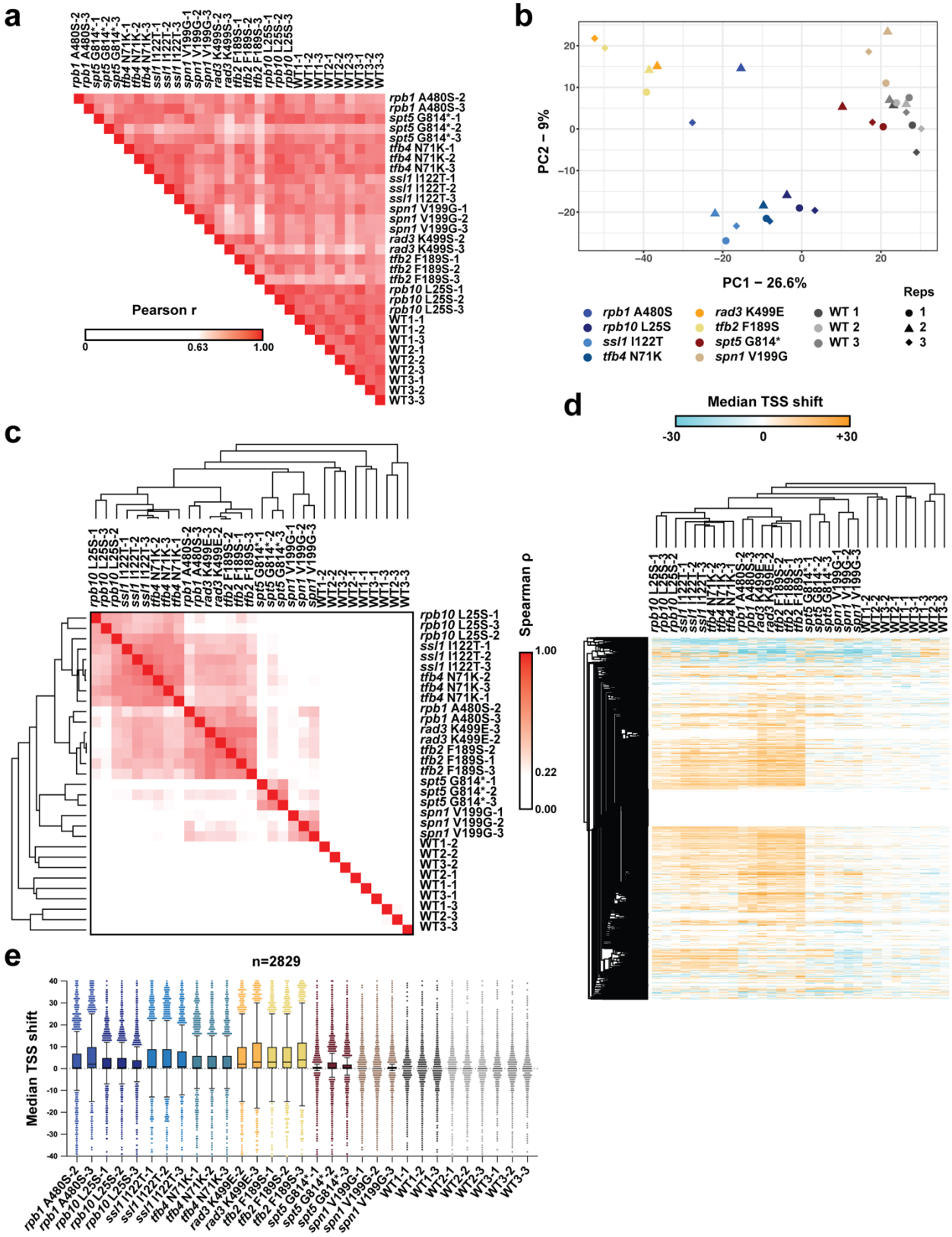
a
Pearson r
0
0.63
1.00
b
PC2 – 9%
PC1 – 26.6%
Reps
1
2
3
rpb1 A480S
rpb10 L25S
ssl1 I122T
tfb4 N71K
rad3 K499E
tfb2 F189S
spt5 G814*
spn1 V199G
WT 1
WT 2
WT 3
c
Spearman ρ
1.00
0.22
0.00
d
Median TSS shift
-30
0
+30
e
n=2829
Median TSS shift

1471

1472 **Figure S5. STRIPE-seq analysis of Δmedian values across individual mutant replicates. a.**
1473 Pearson correlation of individual TSS positions between samples across genome with cutoff per
1474 position set at ≥ 3. **b.** Principal component analysis of Δmedian values across top 2829 genes
1475 qualifying expression cutoff of ≥10 total expression within 401 base analyzed promoter window
1476 for individual sample replicates. **c.** Spearman correlation of Δmedian of top 2829 genes across
1477 all samples and replicates. **d.** Hierarchically clustered heatmap of Δmedian values across all
1478 promoters in individually sequenced samples. **e.** Box-plot analysis of these Δmedian values
1479 amongst all sequenced samples analyzed by Tukey's method.

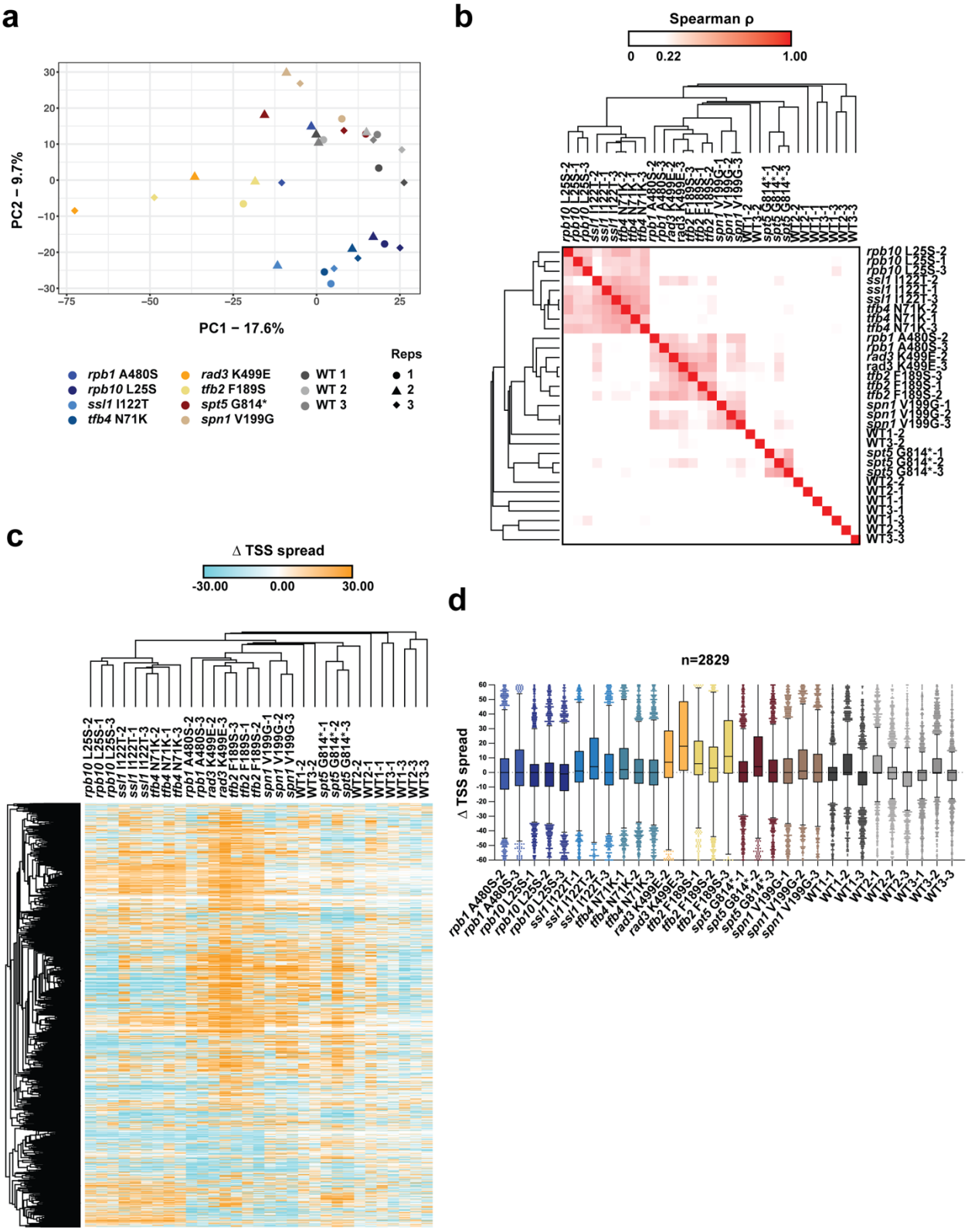


**Figure S6. STRIPE-seq analysis of Δspread values across individual mutant replicates. a.** Principal component analysis of Δspread values across top 2829 genes qualifying expression cutoff of ≥10 within 401 base analyzed promoter window for individual sample replicates. **b.**

1484 Pearson correlation of ∆spread of top 2829 genes across all samples and replicates. **c.**
1485 Hierarchically clustered heatmap of ∆spread values across all promoters in individually
1486 sequenced samples **d.** Box-plot analysis of these ∆spread values amongst all sequenced
1487 samples analyzed by Tukey's method.